

Inhibition of AlkB Nucleic Acid Demethylases: Promising New Epigenetic Targets

Published as part of the *Journal of Medicinal Chemistry* special issue “*Epigenetics 2022*”.

Gemma S. Perry,[†] Mohua Das,[§] and Esther C. Y. Woon^{†,*}

[†]School of Pharmacy, University College London, 29-39 Brunswick Square, London WC1N 1AX, United Kingdom

[§]Lab of Precision Oncology and Cancer Evolution, Genome Institute of Singapore, 60 Biopolis Street, Singapore 138672, Singapore

ABSTRACT: The AlkB family of nucleic acid demethylases is currently of intense chemical, biological and medical interest because of their critical roles in several key cellular processes, including epigenetic gene regulation, RNA metabolism and DNA repair. Emerging evidence suggests that dysregulation of AlkB demethylases may underlie the pathogenesis of several human diseases, particularly obesity, diabetes and cancer. Hence there is strong interest in developing selective inhibitors for these enzymes to facilitate their mechanistic and functional studies, and to validate their therapeutic potential. Herein we review the remarkable advances made over the past twenty years in AlkB demethylase inhibition research. We discuss the rational design of reported inhibitors, their mode-of-binding, selectivity, cellular activity, and therapeutic opportunities. We further discuss unexplored structural elements of the AlkB subfamilies and propose potential strategies to enable subfamily-selectivity. It is hoped that this perspective will inspire novel inhibitor design and advance drug discovery research in this field.

1. INTRODUCTION

The AlkB family of nucleic acid demethylases. The DNA and RNA of all living organisms undergo a diverse range of chemical modifications.¹⁻⁴ Some of these modifications are damaging lesions which can lead to mutations, whilst others are enzyme catalysed with critical roles in a range of biological processes, including the regulation of epigenetic mechanisms, gene expression and RNA functions.¹⁻³ To date, more than 160 distinct nucleic acid base modifications have been reported,⁴ of which the simplest and currently most intensively studied modification is *N*-methylation, where one or more methyl groups are directly added to the nitrogen atom of nucleic acid bases. Through this ingenious mechanism, nature readily generates a repertoire of *N*-methylated bases, thereby rapidly expanding the structural and functional diversity of the four canonical DNA and RNA bases. Some common examples of *N*-methylated bases are given in Table 1. In recent years, it has become increasingly clear that the *N*-methylated bases are present across the three domains of life. It is remarkably prevalent and accounts for more than 60% of all epigenetic modifications in RNA.¹⁻³ Indeed, with the exception of the *N*³ position of guanine, all nucleobase nitrogen positions are known to be methylated. Emerging evidence suggests that the methylation status of these bases are not static, but dynamically regulated by a complex interplay between the DNA/RNA methyltransferases and demethylases, which continuously write and erase the methyl modifications from these bases, respectively.⁵ One important class of nucleic acid demethylases is the AlkB family of iron(II) and 2-oxoglutarate (2OG)-dependent oxygenases,^{6,7} which consist of

Escherichia coli AlkB and nine human homologues, ALKBH1-8 and fat mass and obesity-associated protein (FTO); Figures 1 and 2.

The substrate specificities of AlkB demethylases. From a chemical perspective, the AlkB demethylases is a fascinating class of enzymes because they are able to directly remove *N*-methyl modifications on nucleic acid bases – a reaction that was once thought biologically impossible until landmark discoveries by the research groups of Sedgwick and Hausinger *et al.*, and Falnes *et al.* in 2002,^{8,9} showing that *E. coli* AlkB is able to directly repair *N*¹-methyladenosine (m¹A) and of *N*³-methylcytidine (m³C) methylation damages in bacterial genome *via* an oxidative demethylation reaction (for details, see Section 3 ‘oxidative demethylation by the AlkB subfamilies’). AlkB was subsequently found to repair a variety of DNA and RNA adducts, including *N*³-methylthymidine (m³T), 5-methylcytidine (m⁵C), *N*¹-methylguanosine (m¹G), *N*¹-ethyladenosine (e¹A) and *N*⁶-methyladenosine (m⁶A), as well as exocyclic bridged adducts, such as 1,*N*⁶-ethenoadenosine (εA), 3,*N*⁴-ethenocytidine (εC), *N*²-furan-2-ylmethylguanosine (FF) and *N*²-tetrahydrofuran-2-yl-methylguanosine (HF).¹⁰⁻¹⁵ Following this seminal discovery, six human AlkB homologues ALKBH1-3,

Table 1. Reported nucleic acid substrates for the AlkB demethylases. The AlkB subfamily members demonstrate notable differences in their substrate specificity. The enzymes also exhibit distinct preferences for modified bases in different types of DNA and RNA. The methyl modifications are highlighted in red. Horizontal lines indicate that the base exists, but the reaction does not occur; n.a. denotes not applicable. Abbreviations: m¹A, N¹-methyladenosine; m⁶A, N⁶-methyladenosine; m⁶₂A, N⁶,N⁶-dimethyladenosine; m⁶Am, N⁶,2'-O-dimethyladenosine; e¹A, N¹-ethyladenosine; εA, 1,N⁶-ethanoadenosine; EA, 1,N⁶-ethanoadenosine; m¹G, N¹-methylguanosine; m²G, N²-methylguanosine, e²G, N²-ethylguanosine; 1,N²-εG, 1,N²-ethenoguanosine; FF, N²-furan-2-ylmethylguanosine; HF, N²-tetrahydrofuran-2-yl-methylguanosine; m³C, N³-methylcytidine; m⁴C, N⁴-methylcytidine; m⁵C, 5-methylcytidine; e³C, N³-ethylcytidine; εC, 3,N⁴-ethenocytidine; m³T, N³-methylthymidine; m³U, N³-methyluridine; mcm⁵U, 5-methoxycarbonylmethyluridine; ssDNA, single-stranded DNA; dsDNA, double-stranded DNA; ssRNA, single-stranded RNA; tRNA, transfer RNA; mRNA, messenger RNA; rRNA, ribosomal RNA.

Base	Methylation	DNA		RNA			
		ssDNA	dsDNA	ssRNA	tRNA	mRNA	rRNA
A	m ¹ A	AlkB ^{9,3} ALKBH2 ²³	—	—	AlkB ²⁴ FTO ³³ ALKBH1 ^{19,20} ALKBH3 ²⁸	—	—
	m ⁶ A	AlkB ¹² ALKBH1 ^{21,22} ALKBH4 ³¹	—	—	ALKBH5 ³⁷⁻⁴⁰	—	—
	m ⁶ ₂ A	n.a.	—	—	n.a.	ALKBH5 ⁴⁵	—
	m ⁶ Am	n.a.	n.a.	n.a.	FTO ^{33,34}	n.a.	—
	e ¹ A	AlkB ²³	—	—	n.a.	—	—
	εA	AlkB ¹¹ ALKBH2 ²⁷	—	—	n.a.	—	—
	EA	AlkB ¹⁴	—	—	n.a.	—	—
	—	—	—	—	—	—	—
G	m ¹ G	AlkB ¹⁰	—	AlkB ¹⁸ ALKBH1 ¹⁸ ALKBH3 ¹⁸	n.a.	AlkB ¹⁸ ALKBH1 ¹⁸ ALKBH3 ¹⁸	—
	m ² G	AlkB ¹³	—	—	n.a.	—	—
	e ² G	AlkB ¹³	—	—	n.a.	—	—
	1,N ² -εG	AlkB ¹⁵ ALKBH2 ¹⁵	—	—	n.a.	—	—
	FF	AlkB ¹³	—	—	n.a.	—	—
	HF	AlkB ¹³	—	—	n.a.	—	—
	—	—	—	—	—	—	—
C	m ³ C	AlkB ⁹ ALKBH1 ¹⁶ ALKBH2 ²³	—	—	AlkB ²⁴ ALKBH1 ¹⁸	—	—
	m ³ C	AlkB ¹³	—	—	n.a.	n.a.	—
	m ³ C	AlkB ²⁹ ALKBH2 ²⁹	—	—	ALKBH1 ¹⁹	—	—
	e ³ C	AlkB ¹⁰	—	—	n.a.	—	—
	εC	AlkB ¹¹ ALKBH2 ²⁷	—	—	n.a.	—	—
	—	—	—	—	—	—	—
T	m ³ T	AlkB ¹⁰ ALKBH2 ²⁶	—	—	n.a.	—	—
	—	FTO ³⁵ ALKBH3 ²⁶	—	—	—	—	—
U	m ³ U	n.a.	—	FTO ³²	—	n.a.	—
	mcm ⁵ U	n.a.	—	—	ALKBH8 ⁴	n.a.	—

ALKBH5, ALKBH8 and FTO were similarly identified to possess DNA/RNA demethylase activities. However, none of these human homologues entirely encompass the diverse enzymatic activity of AlkB; instead they exhibit unique substrate specificities. These human homologues also displayed a strong preference for either single-stranded (ss) or double-stranded (ds) DNA/RNA substrates. Table 1 provides a summary of currently known substrates for the AlkB demethylases.

ALKBH1 efficiently demethylates m³C in both ssDNA and ssRNA and possesses DNA lyase activity at abasic sites.^{16,17}

More recently, activity has also been reported against several other substrates, including demethylation of m¹A in both cytoplasmic and mitochondrial tRNAs and m⁶A in bubbled or bulged DNA (instead of ssDNA or dsDNA).^{19,20} It is also able to oxidise m⁵C in tRNAs to generate 5-formylcytidine (f⁵C).¹⁸⁻²² ALKBH2 and ALKBH3 share similar activity profile as ALKBH1, including the ability to demethylate m¹A and m³C in DNA and RNA,¹⁹ however ALKBH2 preferentially demethylate these bases in ssDNA and dsDNA, whereas ALKBH3 strongly prefers ssDNA, ssRNA, mRNA and tRNA.²⁰⁻²⁸ Both ALKBH2 and ALKBH3 are also able to oxidise m⁵C to

5-hydroxymethylcytidine (hm⁵C), ⁵mC and 5-carboxylcytidine (ca⁵C) *in vitro*.²⁹ The activity of ALKBH4 is unique in that it is currently the only subfamily member known to demethylate a protein substrate – a monomethylated site in actin (K84me1). This activity helps regulate the actin-myosin interaction.³⁰ More recently, ALKBH4 was found to demethylate m⁶A base in DNA; the biological significance of this activity is unclear at present.³¹ FTO is the first subfamily member known to demethylate m⁶A in mRNA; notably, m⁶A is a highly-prevalent epigenetic modification in mRNA which critically regulates all major aspects of mRNA functions, including mRNA stability, alternative splicing and translational efficiency.³² In recent years, a number of additional RNA substrates for FTO have been uncovered, including m¹A in nuclear and cytoplasmic tRNA, which is important for controlling translation efficiency, and N⁶,2'-O-dimethyladenosine (m⁶Am) – a major modified nucleotide found at the 5' cap on polyadenylated RNA that regulates the mRNA integrity, stability and resistance to decapping.^{33,34} FTO also catalyses the direct removal of m³T and N³-methyluridine (m³U). In the case of m³T, FTO exhibits a strong preference for ssDNA over dsDNA, whereas for m³U, FTO favours ssRNA over dsDNA.^{35,36} ALKBH5 is the only other human enzyme (besides FTO) currently known to demethylate m⁶A in mRNA. However FTO and ALKBH5 likely target different m⁶A-containing mRNA transcripts,³⁷⁻⁴⁰ since they exhibit distinct physiological functions and are associated with different human diseases, *e.g.* FTO is implicated in obesity whereas ALKBH5 is linked to colon cancer.⁴¹⁻⁴⁴ Recent evidence suggests that ALKBH5 likely also demethylates the di-methylated adenosine base, N⁶,N⁶-dimethyladenosine (m⁶₂A), which is present in ribosomal RNA as a normal component of the ribosome that assists in translation.⁴⁵ ALKBH8 appears to be highly exclusive in its substrates. It specifically catalyses the hydroxylation of 5-methoxycarbonylmethyluridine (mcm⁵U) at the wobble position of tRNA to form a stable hydroxylated base (*S*)-5-methoxycarbonylhydroxymethyluridine (mchm⁵U) which, notably, does not spontaneously demethylate, unlike most hydroxylated bases produced by other AlkB demethylases.⁴⁶ The physiological significance of this reaction is unclear, although modified nucleosides in the tRNA anticodon loop in many cases contribute to reading frame maintenance and stabilization of codon-anticodon pairing.

The catalytic activity of ALKBH6 and ALKBH7 is unknown at present, however it has been suggested that ALKBH6 likely possesses potential activity against modified RNA bases. This is based on observations that ALKBH6 has a highly positively-charged protein surface, a relatively high isoelectric value, and is localised in both the nucleus and cytoplasm.⁴⁷ Consistent with this hypothesis, recent studies found that *Arabidopsis* alkbh6 protein can bind to both m⁶A-labelled and m⁵C-labelled RNAs.⁴⁷ Whether or not human ALKBH6 exhibits demethylase activity against these methylated bases remained to be investigated. Recent crystallographic analysis also suggests that ALKBH7 likely demethylates proteins rather than nucleic acids due to the absence of nucleotide recognition lid domain (NRL),⁴⁸ which is essential for binding to nucleobase (for details, see Section 2 'structural comparisons of AlkB demethylases for rational

drug design'). Although significant progress has been made in uncovering a diversity of nucleic acid (and protein) substrates catalysed by the AlkB demethylases, it is likely that the full extent of their activity has not yet been defined.

The role of AlkB demethylases in biology and human diseases. The identification of substrates for various AlkB demethylases is a major step toward a complete understanding of the biological functions of these fascinating enzymes. A number of excellent reviews are currently available that discuss their epigenetic mechanisms and therapeutic potentials in detail.⁴⁹⁻⁵² It has become increasingly clear that the AlkB subfamilies are associated with a range of human diseases. FTO, in particular, is strongly linked to obesity,⁴¹⁻⁴³ type II diabetes,^{53,54} Alzheimer's disease^{55,56} and non-alcoholic steatohepatitis (NASH),⁵⁷ whereas ALKBH1 is implicated in gastric cancer and glioblastoma.^{58,59} Emerging evidence further suggests that both ALKBH2 and ALKBH3 function as DNA repair enzymes *in vivo* and their overexpression likely promotes tumorigenesis in humans.⁶⁰⁻⁶³ For instance, ALKBH2 is highly expressed in bladder cancer⁶⁰ whilst ALKBH3, also known as prostate cancer antigen-1 (PCA-1), contributes to the progression of pancreatic cancer, non-small cell lung cancers, renal cell carcinoma, and is currently being targeted for the treatment of prostate cancer.⁶¹⁻⁶³ There is also evidence that ALKBH5 is involved in spermatogenesis and colon cancer.⁴⁴ More recently, ALKBH7 and ALKBH8 are reported to be linked to prostate cancer and bladder cancer, respectively, and could be potential targets for the treatment of these cancers.⁶⁴⁻⁶⁶

The strong physiological links between AlkB demethylases and several human diseases has stimulated intense interest, in both academia and the pharmaceutical industry, to develop small molecule inhibitors for these enzymes to facilitate their structural, mechanistic and functional studies, with a longer-term view to validating their therapeutic potential. Recently, Cheng *et al.*⁶⁷ published an excellent review on small-molecule inhibitors of AlkB demethylases, focusing on selective compounds. To date, there has not been a comprehensive discussion of inhibition studies of this class of enzymes, which would greatly facilitate rational drug design and inspire the development of next generation inhibitors. In this perspective, we review the remarkable advances made over the past twenty years in improving the potency and selectivity of AlkB demethylases inhibitors. We discuss the rational design of most, if not all, reported inhibitors, their mode-of-binding, selectivity, cellular activity, and therapeutic opportunities. We further discuss subfamily-specific structural elements of the AlkB demethylases and suggest potential strategies to enable subfamily-selectivity. We hope that this work will stimulate further inhibition studies of these medically-important enzymes and advance the development of novel epigenetic therapies.

2. STRUCTURAL COMPARISONS OF ALKB DEMETHYLASES FOR RATIONAL DRUG DESIGN

To date, more than 100 crystal structures of the AlkB subfamily members have been reported, providing rich structural insights into their ligand/substrate recognition and catalytic mechanisms. The wealth of structural information

Table 2. Reported crystal structures for the AlkB demethylases. The substrates, co-substrate and active site metal for the co-crystal structures are indicated. Where inhibitor is present, this is indicated in bold and numbered as in the main text.

Protein	Species	PDB ID	Resolution (Å)	Sequence	Ligands	Active site metal	
AlkB	<i>Escherichia coli</i>	4NIJ ⁷⁰	1.62	12-216	m ⁶ A-dsDNA, 2OG	Mn(II)	
		4NIG ⁷⁰	1.52		m ⁶ A-dsDNA, 2OG	Mn(II)	
		4NID ⁷⁰	1.58		m ⁶ A-dsDNA, 2OG	Mn(II)	
		4NIH ⁷⁰	1.37		m ⁶ A-dsDNA, 2OG	Mn(II)	
		3KHC ⁷¹	2.20	1-216	m ¹ G-ssDNA, 2OG	Co(II)	
		3KHB ⁷¹	2.90		2OG	Co(II)	
		6Y0Q ⁷²	1.75		m ¹ A-T, 2OG	Fe(II)	
		6YPV ⁷²	2.10		2OG	Fe(II)	
		3I49 ⁷³	1.60	12-216	T-m ³ C-T, 2OG	Fe(II)	
		3I2O ⁷³	1.70		T-m ¹ A-T, 2OG	Fe(II)	
		3I3M ⁷³	1.50		T-m ³ C-T, 2OG	Mn(II)	
		3I3Q ⁷³	1.40		2OG	Mn(II)	
		3BKZ ⁸⁴	1.65	14-214	dsDNA, 2OG	Mn(II)	
		3BI3 ⁸⁴	1.90	13-213	m ¹ A-dsDNA, 2OG	Mn(II)	
		3BIE ⁸⁴	1.68	13-214	m ¹ A-dsDNA, 2OG	Mn(II)	
		2FDH ⁸⁵	2.10	12-216	T-m ¹ A-T, 2OG	Mn(II)	
		2FDJ ⁸⁵	1.80		T-m ¹ A-T, 2OG, Succinate 8	Fe(II)	
		2FDJ ⁸⁵	2.10		Succinate 8	Fe(II)	
		2FDG ⁸⁵	2.20		T-m ¹ A-T, Succinate 8	Fe(II)	
		2FDK ⁸⁵	2.30		T-m ¹ A-T, 2OG	Fe(II)	
		2FD8 ⁸⁵	2.30		T-m ¹ A-T, 2OG	Fe(II)	
		2FDF ⁸⁵	2.10		T-m ¹ A-T, 2OG	Co(II)	
		3T3Y ¹¹²	2.00		19	Fe(II)	
		3T4V ¹¹²	1.73		5	Fe(II)	
		3T4H ¹¹²	1.65		2	Fe(II)	
		3O1U ¹¹⁸	1.54		dsDNA, Succinate 8	Fe(II)	
		3O1M ¹¹⁸	1.75		m ³ C-dsDNA, 2OG	Mn(II)	
		3O1R ¹¹⁸	1.77		dsDNA, 2OG	Mn(II)	
		3O1P ¹¹⁸	1.51		εA-dsDNA, 2OG	Mn(II)	
		3O1V ¹¹⁸	1.90	dsDNA, Succinate 8	Fe(II)		
		3O1T ¹¹⁸	1.48	dsDNA, Succinate 8	Fe(II)		
		3O1O ¹¹⁸	1.92	dsDNA, 2OG	Mn(II)		
		3O1S ¹¹⁸	1.58	dsDNA, Succinate 8	Fe(II)		
		4JHT ¹²⁶	1.18	IOX1 32	Mn(II)		
		4RFR ¹⁴⁰	1.50	14-216	Rhein 52	Mn(II)	
		4ZHN	1.33	12-216	T-m ¹ A-T, 2OG	Co(II)	
		5ZMD ⁸⁰	3.30	37-499	m ⁶ A-dsDNA, NOG 1	Mn(II)	
		3LFM ⁸⁶	2.50	32-505	m ³ T, NOG 1	Fe(II)	
		4CXW ¹⁰⁸	3.10		Lipof F 23	Ni(II)	
		4CXY ¹⁰⁸	2.65		22	Ni(II)	
		4CXX ¹⁰⁸	2.76		24	Ni(II)	
		6AKW ¹⁰⁷	2.20	32-502	FB23 60 , 2OG	--	
		4IE0 ¹¹⁴	2.53	32-505	2,4-PDCA 15	Zn(II)	
		4IE5 ¹¹⁴	1.95		20	Zn(II)	
		4IE6 ¹¹⁴	2.50		IOX3 35	Zn(II)	
		4IDZ ¹¹⁴	2.46		NOG 1	Ni(II)	
		4IE7 ¹¹⁴	2.60	32-503	Rhein 52 , Citrate 7	Zn(II)	
4IE4 ¹¹⁴	2.50	IOX1 32	Zn(II)				
4QKN ¹⁴¹	2.20	32-503	MA 59 , NOG 1	Mn(II)			
4ZS3 ¹⁴³	2.45	32-505	67 , 2OG	Mn(II)			
4ZS2 ¹⁴³	2.16		Fluorescein 65 , 2OG	Mn(II)			
5DAB ¹⁴⁴	2.10	32-159	CDPCB 75 , 2OG	Fe(II)			
6AK4 ¹⁴⁷	2.80		Entacapone 87	Zn(II)			
6AEJ ¹⁴⁷	2.80		91	Zn(II)			
5F8P	2.20	32-502	CHTB 85 , 2OG	Fe(II)			
4QHO	2.37	32-505	<i>N</i> -[3-hydroxy-6-(naphthalen-1-yl)pyridin-2-yl] carbonyl glycine	Zn(II)			
AlKBH1	<i>Homo sapiens</i>	6IE3 ²¹	1.97	1-389	--	Mn(II)	
		6IE2 ²¹	2.80		2OG	Mn(II)	
	<i>Mus musculus</i>	6KSF ²²	2.40	20-355	dsDNA, Succinate 8	--	
		6IMA ²²	2.59	37-369	Citrate 7	--	
		6L94 ²⁴	3.10	4-389	--	Fe(II)	
		4MG2 ⁷⁵	2.30	56-258	dsDNA	Mg(II)	
		4MGT ⁷⁵	2.60		dsDNA	Mg(II)	
	<i>Homo sapiens</i>	3RZJ ⁷⁶	2.50	56-261	m ³ C-dsDNA, 2OG	Mn(II)	
		3RZK ⁷⁶	2.78		εA-dsDNA, 2OG	Mn(II)	
		3RZL ⁷⁶	2.60		dsDNA	--	
		3RZG ⁷⁶	1.62		dsDNA	--	
		3RZH ⁷⁶	2.25		m ³ C-dsDNA	--	
		3SSA ⁷⁶	1.70		56-258	dsDNA, 2OG	Mn(II)
		3S57 ⁷⁶	1.60		dsDNA, 2OG	Mn(II)	
		3RZM ⁷⁶	3.06		56-260	dsDNA	--
		3H8O ⁷⁷	2.00		56-261	m ¹ A-dsDNA	--
		3H8R ⁷⁷	1.77			m ⁶ A-dsDNA	--
3H8X ⁷⁷		1.95	m ³ C-dsDNA			--	
3BTZ ⁸⁴		3.00	57-258			dsDNA	--
<i>Homo sapiens</i>	3BTX ⁸⁴	2.00	56-258	dsDNA	Mg(II)		
	3BUC ⁸⁴	2.59		m ¹ A-dsDNA, 2OG	Mn(II)		
	3BTY ⁸⁴	2.35		m ¹ A-dsDNA	--		
	3BU0 ⁸⁴	2.50		dsDNA, 2OG	Mn(II)		
	2IUW ⁷⁸	1.50		62-286	2OG	Fe(II)	
	<i>Homo sapiens</i>	4O7X ³⁸		1.78	66-292	--	Mn(II)
		4NRP ³⁸		1.80		NOG 1	Mn(II)
		4NRO ³⁸		2.30		NOG 1	Mn(II)
4NRQ ³⁸		2.50	2,4-PDCA 15	Mn(II)			
4NRM ³⁸		2.17	Citrate 7	--			
4O61 ³⁹		1.90	74-294	Citrate 7		--	
4OCT ³⁹		2.28	2OG	Mn(II)			
4NJ4 ⁸²		2.02	66-292	IOX3 35		Mn(II)	
<i>Danio rerio</i>	4NPM ¹¹⁹	1.80	38-287	Succinate 8	Mn(II)		
	4NPL ¹¹⁹	1.65		2OG	Mn(II)		
<i>Homo sapiens</i>	4QKB ⁴⁸	2.60	17-215	2OG	Mn(II)		
	4QKF ⁴⁸	1.99		NOG 1	Mn(II)		
<i>Homo sapiens</i>	4QKD ⁴⁸	1.35	2OG	Mn(II)			
	3THT ⁷⁹	3.01	25-355	2OG	Mn(II)		
<i>Homo sapiens</i>	3THP ⁷⁹	3.20	2OG	Mn(II)			

further enables structure-based and computationally-aided inhibitor design (for excellent review, see ref. 68 and 69). In this section we focus on the unique structural features of the AlkB subfamily members that may be exploited for rational drug design. Table 2 provides a list of all available X-ray crystal structures of the AlkB demethylases to date. To date, all AlkB subfamily members have been structurally characterised, with the exception of ALKBH4 and ALKBH6.⁷⁰⁻⁸⁰ Figure 2 provides representative views of the crystal structures of AlkB demethylases in complex with either 2OG co-substrate or its catalytically-inert analogue NOG (*N*-oxalylglycine).

The double-stranded β-helix. As is characteristic of most Fe(II)/2OG-dependent oxygenases, the AlkB demethylases possess a central catalytic domain, which is formed by eight β-strands that fold into a double-stranded β-helix (DSBH) structure, commonly known as the 'jelly-roll' fold (Figures 1 and 2).⁸¹ Sandwiched within the DSBH fold are two highly-conserved structural elements that are essential for oxidative demethylase activity. 1) The 'HXD...H' iron-binding motif which consists of a triad of two histidine and one aspartate residue. This motif is responsible for binding the iron in a tridentate manner. 2) The 'R...R' 2OG-binding motif, which stabilises the binding of 2OG co-substrate *via*

two salt-bridge interactions between the C-1 and C-5 carboxylate oxygens of 2OG and the arginine residues.

From an inhibitor design perspective, it is important to note that all residues involved in iron and 2OG binding are highly conserved across the AlkB subfamily members – indeed structural alignment studies revealed high levels of structural similarities of the 2OG-binding sites amongst the AlkB subfamilies, with almost identical topology and folding patterns. Hence, it is challenging to design selective inhibitors based on the 2OG-binding site alone. Nevertheless, as will be discussed in Section 4.1 ‘inhibitors that complex with iron in the 2OG-binding site’, a number of fairly selective AlkB and FTO inhibitors, that binds to the 2OG-binding site alone, have emerged in recent years, suggesting that it is possible to achieve selective inhibition by targeting this motif exclusively.

Secondary structural elements surrounding the DSBH. The AlkB demethylases also contain additional structural elements surrounding the DSBH motif, such as the *N*-terminal extension (NTE), *C*-terminal domain (CTD) and nucleotide-recognition lid (NRL), which not only help to stabilise the central jelly-roll fold, but also contribute to important structural differences amongst the AlkB subfamily members (for details of domain architecture, see Figure 1B). Structural and bioinformatic studies revealed that, with the exception of ALKBH7, all AlkB homologues possess a NRL which consists of two β -hairpin-like loop structures known as Loop 1 and Loop 2.^{82,83} Together they form a lid over the DSBH active site and constitutes the substrate-binding site. It is increasingly clear that Loop 1 determines single-stranded versus double-stranded substrate preference.²⁵ Loop 2, on the other hand, provides residues for the recognition and binding of specific nucleotide substrates.²⁵ Hence both loop structures are crucial for determining the substrate specificity of the AlkB subfamilies.

The NRL also provides residues for flipping of the methylated base into the active site. Recent structural study by He *et al.* provided unprecedented, detailed views of the molecular recognition of different duplex nucleotide substrates by AlkB and ALKBH2.⁸⁴ The authors showed that the NRL of ALKBH2 flips the methylated base out of the dsDNA helix and fills the vacant space by a hydrophobic amino acid residue, in a manner similar to DNA glycosylases; whereas the NRL of AlkB squeezes together the bases flanking the flipped-out base to maintain the base stack.^{84,85} Subsequent work by Chai *et al.* found that the Loop 1 of FTO sterically hinders the access of dsDNA to the substrate-binding site, thus rationalising the preference of FTO for ssRNA over dsDNA substrates.⁸⁶ More recently, the Loop 1 of ALKBH1 was found to assume a fully extended conformation; this likely prevents autonomous base-flipping which may account for the inability of ALKBH1 to demethylate dsDNA.^{16,21,22} Interestingly, the NRL sequence in ALKBH8 is largely disordered, likely indicating a degree of flexibility in substrate requirements. ALKBH7, on the other hand, lacks the NRL, which is essential for binding to nucleobases, implying that ALKBH7 likely do not act on nucleic acid substrates.⁴⁸ Moreover, ALKBH7 exhibits a large, solvent-exposed groove that potentially permits the binding of relatively larger protein substrates.

Besides the NRL, a number of AlkB subfamilies contain additional protein domains which provide further structural and functional variations (Figure 1B). For instance, FTO contains a unique CTD which possibly helps stabilise the conformation of the NTD, thus is important for its catalytic activity.⁸⁶ ALKBH5 possesses an *N*-terminal alanine-rich sequence (consisting of 19 alanine residues) which is likely responsible for its localisation to nuclear speckles.³⁷ ALKBH7 contains an *N*-terminal mitochondrial targeting sequence (MTS) which directs its localisation to mitochondria where it regulates the processing of polycistronic mitochondrial RNAs and mitochondrial activity.^{87,88} Interestingly, in addition to being a demethylase, ALKBH8 also contains a *C*-terminal methyltransferase domain (MT) which serves to catalyse the methylation of 5-carboxymethyluridine (cm⁵U) at the wobble position of the anticodon loop in tRNA to form 5-methoxycarbonylmethyluridine (mcm⁵U).⁸⁹ The methyltransferase activity of ALKBH8 is likely facilitated by an *N*-terminal RNA recognition motif (RRM) which provides for specific binding to tRNA.

It is important to note that the NRL is an exclusive structural feature of the AlkB subfamilies, which is not present in other Fe(II)/2OG-dependent oxygenases. Hence, the NRL domain could potentially be exploited to achieve selective inhibition of AlkB demethylases over other Fe(II)/2OG-dependent oxygenases. The many other subfamily-specific structural elements identified, such as the CTD in FTO and the methyltransferase domain in ALKBH8, should also enable selective targeting of specific AlkB subfamily members.

3. OXIDATIVE DEMETHYLATION BY THE ALKB SUBFAMILIES

As discussed above, all AlkB subfamily members contain a DSBH catalytic domain which enables oxidative demethylation of a range of substrates. Pioneering studies by Hausinger *et al.*,^{69,90} Schofield *et al.*,^{91,92} Krebs *et al.*,⁹³ He *et al.*^{32,94} and many others (*e.g.* ref 72, 95-97) have provided extensive crystallographic, kinetic, spectroscopic and biochemical evidences for the catalytic mechanisms of AlkB demethylases and other Fe(II)/2OG-dependent oxygenases. A number of excellent reviews are available which describe the oxidative demethylation mechanism of AlkB demethylases in detail.⁹⁸⁻¹⁰² In brief, the current consensus is that nucleic acid demethylation proceeds through an ordered, sequential mechanism as shown in Figure 1C. It likely begins with the coordination of active site Fe(II) to His-Asp-His triad and to three water molecules (enzyme resting state **A**; Figure 1C). i) The 2OG co-substrate then chelates to Fe(II) in a bidentate manner, displacing the two metal-bound water molecules that are *trans* to the proximal histidine and aspartate residues to form a Fe(II)-2OG complex **B**. ii) Subsequent binding of the methylated substrate to the substrate-binding site (which is in close proximity to the Fe(II) centre) weakens the binding of the remaining water molecule to Fe(II) and displaces it, iii) creating a site for the binding of a dioxygen molecule to form a Fe(III)-superoxo intermediate **C**. iv) This intermediate is highly unstable. It rapidly collapses to form an Fe(IV)-bicyclic species **D** which, in

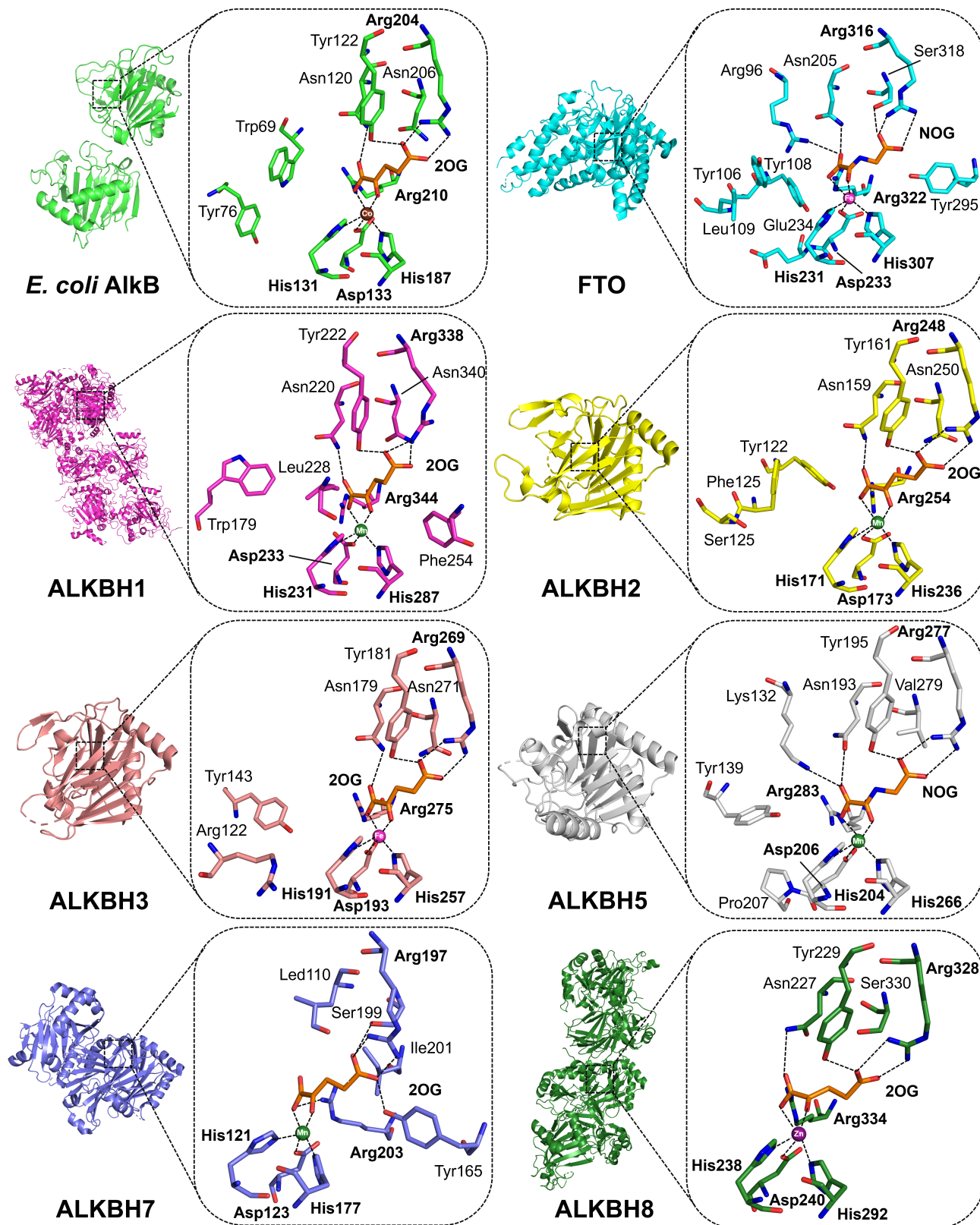


Figure 2. Views of the crystal structures of AlkB demethylases in complex with co-substrate 2OG or NOG. Close-up views show the interactions of residues in the 2OG-binding site with 2OG or NOG. The highly conserved His-Asp-His iron binding triad and the Arg residues in the 'R...R' motif are indicated in bold. The X-ray crystal structures of ALKBH4 and ALKBH6 have not been solved. PDB IDs: *E. coli* AlkB (3KHC),⁷¹ FTO (3LFM),⁸⁶ ALKBH1 (6IE2),²¹ ALKBH2 (3BU0),⁸⁴ ALKBH3 (2IUW),⁷⁸ ALKBH5 (4NRP),³⁸ ALKBH7 (4QKD),⁴⁸ ALKBH8 (3THT).⁷⁹

generate succinate and a highly reactive Fe(IV)-oxo species **E**. vi) In the final steps of the catalytic cycle, intermediate **E** abstracts a hydrogen atom from the substrate to produce an Fe(III)-OH intermediate **F**, vii) followed by hydroxyl radical rebound to form the hydroxylated product **G**. viii) The product and succinate then dissociate from the enzyme and the vacant Fe(II) ligand positions are again occupied by three water molecules to regenerate the enzyme resting state **A**. In most cases, the hydroxylated product is unstable and undergoes spontaneous fragmentation to generate formaldehyde and the demethylated product.

4. SMALL MOLECULE INHIBITORS OF ALKB DEMETHYLASES

Over the past decades, we have witnessed tremendous advances in the development of AlkB demethylase inhibitors. Inhibition work is massively facilitated by the development of a range of demethylase assay methods and the availability of plentiful high-resolution crystal structures, which provides a wealth of structural information to enable structure-based and computationally-guided inhibitor design. In this section, we discuss studies on the inhibition of AlkB demethylases. We critically reviewed most, if not all, reported small-molecule AlkB demethylase inhibitors, focusing on their rational design, mode of binding, selectivity, cellular activity, and therapeutic potential. The vast majority of identified inhibitors can be organised into three broad classes based on their mode of binding, namely 1) inhibitors that complexed with iron in the 2OG-binding site, 2) inhibitors that bind exclusively to the substrate-binding site, and 3) inhibitors with undetermined mode of binding.

4.1 Inhibitors that complex with iron in the 2OG-binding site

Most of the early AlkB demethylases inhibitors are 2OG-competitive inhibitors. A characteristic feature of inhibitors from this class is that they carry a metal-binding warhead (*e.g.* oxalyl, pyridyl carboxylate and acylhydrazine groups) which enables them to chelate to active site metal in the 2OG-binding site, usually in a bidentate manner akin to 2OG. These inhibitors were largely discovered through high-throughput screening, Dynamic Combinatorial Mass Spectrometric (DCMS) methods^{103,104,111,112,136} and structure-based design. Tables 3-6 summarise all the available IC₅₀ data and chemical structures of this class of inhibitors.

***N*-Oxalylglycine (NOG) 1** is an amide analogue of 2OG, wherein the C-3 of 2OG is replaced with a nitrogen atom. Being a close structural analogue of 2OG, NOG is able to inhibit a diverse range of Fe(II)/2OG-dependent oxygenases, although its potency against different enzymes varies. For instance, under similar assay conditions, NOG inhibits PHD2 (IC₅₀ = 6.2 μM) more strongly than KDM4A (IC₅₀ = 250 μM; Table 3).¹⁰⁵ Similarly, within the AlkB subfamilies, NOG showed significantly greater inhibition for FTO (IC₅₀ = 36.5 μM) than for ALKBH5 (IC₅₀ = 145.2 μM; Table 3).¹⁰⁶ The observed differences in inhibitory activity likely reflects the varying affinities of 2OG for the Fe(II)/2OG-oxygenases. The co-crystal structures of NOG bound to several AlkB demethylases, including ALKBH1,²² ALKBH5,³⁸ ALKBH7,⁴⁹ and

FTO have been determined.⁷⁹ These structures invariably show NOG forming bidentate chelation to the active site iron through its C-1 carboxylate and C-2 ketone oxygens, in a manner analogous to 2OG (Figure 2). However, unlike 2OG, NOG is unable to initiate the oxidative demethylation process when bound to AlkB demethylases (and other Fe(II)/2OG-oxygenases), presumably because it is less susceptibility to attack by the Fe(III)-superoxo species (for details, see Section 3 'oxidative demethylation by the AlkB subfamilies'; Figure 1C). NOG merely forms a catalytically-inert complex which blocks 2OG binding, hence this inhibitor is widely used in crystallographic studies to produce stable enzyme-substrate complexes. It has also been used extensively in functional studies of Fe(II)/2OG-dependent oxygenases, for instance to investigate the roles of FTO in epigenetic gene regulations^{40,107} and to induce pseudohypoxia through inhibition of PHDs (HIF prolyl hydroxylases; a key oxygen-sensing enzyme crucial for cellular hypoxic response).¹⁰⁸⁻¹¹⁰ For cell-based and animal studies, the dimethyl ester prodrug of NOG, dimethyl oxalylglycine (DMOG), which is more cell-penetrant is used; DMOG efficiently penetrates the cells where it is hydrolysed back to NOG by cellular carboxylesterases.¹⁰⁸

One major concern with the use of DMOG/NOG in cellular studies, however, is that they likely cause indiscriminate, pan-inhibition of Fe(II)/2OG-dependent oxygenases. Hence, at least some of the observed biological effects of NOG would be due to concurrent inhibition of several Fe(II)/2OG-dependent oxygenases. Care should therefore be taken when interpreting results from these studies. It is interesting to note that, although NOG was independently developed through medicinal chemical effort, this compound, as well as DMOG, were subsequently found to be present in rhubarb (*Rheum rhabarbarum*) and spinach (*Spinach oleracea*) leaves,¹¹¹ suggesting that they might have a natural role in regulating the activity of Fe(II)/2OG-dependent oxygenases. Whether or not they exist naturally in humans and animals remain to be investigated, although current studies found no detectable levels of NOG and DMOG in *E. coli* and human embryonic kidney cell extracts.

***N*-Oxalyl amino acids.** Early inhibition work on *E. coli* AlkB suggests that substitution at the C- α position of NOG can lead to an increase in potency and selectivity.^{112,113} One such study employed a DCMS approach, linking disulfide-based dynamic combinatorial chemistry with non-denaturing mass spectrometric analyses, which led to the identification of *N*-oxalyl-*L*-cysteine derivatives **2-6** as potent inhibitors of AlkB (Table 3).¹¹² Some of these inhibitors exhibit significant selectivity (200-2000-fold) for AlkB over other physiologically-important human Fe(II)/2OG-dependent oxygenases, such as PHD2 and PHF8 (PHD finger protein 8; linked to midline defects), which is highly encouraging because it demonstrated that AlkB and, by implication, other AlkB demethylases are amenable to potent and selective inhibition by NOG analogues.¹¹² This work further revealed a distinct preference of AlkB for the *L*-enantiomers of *N*-oxalyl amino acids over the *D*-counterparts. Notably, the *D*-enantiomers are generally favoured by other Fe(II)/2OG-oxygenases, including factor inhibiting HIF (FIH),⁸¹

Table 3. Available inhibition data for *N*-oxalylglycine analogues and endogenous metabolites against AlkB demethylases and other Fe(II)/2OG-dependent oxygenases. The metal chelating motif is highlighted in red. Horizontal lines indicate that no inhibition data are available.

Code	IC ₅₀ /μM					Other Fe(II)/2OG-oxygenases	Chemical structure
	AlkB	FTO	ALKBH2	ALKBH3	ALKBH5		
1	108.3 ¹⁰⁶	36.5 ¹⁰⁶	124.7 ¹⁰⁶	96.8 ¹⁰⁶	145.2 ¹⁰⁶ 25.85 ³⁸	FIH (0.84) ¹¹⁰ PHD1 (2.1) ¹⁰⁵ PHD2 (6.2) ¹⁰⁵ KDM4A (250) ¹⁰⁵ KDM4C (500) ¹⁰⁵	 1 NOG
2	5.2 ¹¹²	-	-	-	-	PHD2 (>1000) ¹¹² PHF8 (>1000) ¹¹²	 2 R =
3	48 ¹¹²	-	-	-	-	-	 3 R =
4	50.4 ¹¹²	-	-	-	-	-	 4 R =
5	0.5 ¹¹²	-	-	-	-	PHD2 (>1000) ¹¹² PHF8 (>1000) ¹¹²	 5 R =
6	5.4 ¹¹²	-	-	-	-	PHD2 (>1000) ¹¹² PHF8 (>1000) ¹¹²	 6 R =
7	-	300 ¹¹⁴	-	-	488 ³⁹ 627.9 ³⁸	FIH (850) ¹¹⁶ PHD1 (6300) ¹¹⁶ PHD2 (4800) ¹¹⁶ PHD3 (550) ¹¹⁶	 7 Citrate
8	-	370 ¹¹⁴	-	-	30 ³⁸	FIH (>10000) ¹¹⁶ PHD1 (830) ¹¹⁶ PHD2 (510) ¹¹⁶ PHD3 (570) ¹¹⁶	 8 Succinate
9	-	>1000 ¹¹⁴	-	-	-	FIH (5000) ¹¹⁶ PHD1 (>10000) ¹¹⁶ PHD2 (>10000) ¹¹⁶ PHD3 (>10000) ¹¹⁶	 9 Isocitrate
10	-	150 ¹¹⁴	-	-	-	FIH (>10000) ¹¹⁶ PHD1 (120) ¹¹⁶ PHD2 (80) ¹¹⁶ PHD3 (60) ¹¹⁶	 10 Fumarate
11	-	>1000 ¹¹⁴	-	-	-	FIH (>10000) ¹¹⁶ PHD1 (>10000) ¹¹⁶ PHD2 (>10000) ¹¹⁶ PHD3 (>10000) ¹¹⁶	 11 Malate
12	5100 ¹²²	320 ¹¹⁴	424 ¹²³	8300 ¹²²	-	FIH (1500) ¹²³ PHD2 (7300) ¹²³ KDM4A (24) ¹⁰⁵ KDM4C (79) ¹⁰⁵	 12 R-2HG R¹ = H, R² = OH
13	8600 ¹²²	>1000 ¹¹⁴	150 ¹²³	24300 ¹²²	-	FIH (189) ¹²³ PHD2 (419) ¹²³ KDM4A (26) ¹⁰⁵ KDM4C (97) ¹⁰⁵	 13 S-2HG R¹ = OH, R² = H
14	120 ¹²⁴	-	-	-	-	-	 14 (±) 2MG R = SH

JmjC KDMs,¹¹³ and FTO¹¹⁴ (for details, see Section on 'quinoline and isoquinoline carboxamide derivatives'; Table 5); thus chirality could provide a useful strategy to drive selectivity towards AlkB. In designing AlkB inhibitors as potential antibacterial agents, it is important to appreciate that the effects of AlkB inhibition could potentially be compensated by a number of other *E. coli* enzymes with overlapping substrate specificities, such as DNA glycosylases AlkA, AlkC and MUG,¹¹⁵ thus a multi-targeted approach may be needed.

Endogenous metabolites. Apart from being an obligatory substrate for AlkB demethylases, 2OG is also a key intermediate in the tricarboxylic acid (TCA) cycle. Several of the TCA cycle intermediates, such as citrate **7**, succinate **8**, isocitrate **9**, fumarate **10** and malate **11** have been reported to competitively inhibit FTO,¹¹⁴ ALKBH2, ALKBH3, ALKBH5^{38,39} and a broad range of other Fe(II)/2OG-dependent oxygenases, including FIH, PHD1-3 and KDM4E,¹¹⁶ with potency's ranging from high

micromolar to millimolar range; Table 3. For excellent reviews, see ref. 117 & 125. It is increasingly clear that AlkB demethylases (and other Fe(II)/2OG-oxygenases) exhibit varying affinities for the TCA cycle intermediates, thus their sensitivity to depletion of specific co-substrates, varies widely. This finding has prompted considerable interest in understanding the physiological connection between the TCA metabolites and AlkB demethylases, as well as their relevance to human diseases.

Multiple crystal structures of citrate and succinate bound to AlkB demethylases have been solved; some examples include FTO-citrate complex (PDB ID: 4IE7),¹¹⁴ ALKBH5-citrate complex (PDB ID: 4NRM),³⁸ AlkB-succinate complex (PDB IDs: 2FDJ, 3O1S)^{85,118} and ALKBH5-succinate complex (PDB ID: 4NPM).¹¹⁹ Collectively, these co-crystal structures revealed that citrate, succinate and, by inference, other structurally-related TCA cycle intermediates occupy the 2OG-binding site in a manner competitive with 2OG. Citrate **7**, for instance, coordinates to active site iron in a monodentate manner through one of its carboxylate groups (the remaining iron coordination site, that would otherwise be occupied by the C-1 carboxylate of 2OG, is occupied by a water molecule).^{38,114} The second carboxylate of citrate interacts with the conserved arginine, whilst the third carboxylate forms a hydrogen-bond to an asparagine residue. Likewise, succinate **8** coordinates to active site metal through one of its carboxylate groups in a monodentate manner, analogous to citrate binding (Figure 3A). Citrate **7**, succinate **8** and fumarate **10** also bind in a similar manner to KDM4A and FIH, as apparent from the crystal structures of KDM4A-succinate (PDB ID: 2Q8D),¹²⁰ FIH-succinate (PDB ID: 2CGN)¹²¹ and FIH-fumarate (PDB ID: 2CGO).¹²¹ Thus, despite lacking an oxalyl group, these TCA cycle intermediates are able to bind competitively to active site iron, albeit weakly.

In addition to the TCA cycle intermediates, other structurally-related endogenous metabolites, notably 2-hydroxyglutarate (2HG; both the *R*- and *S*-enantiomeric forms **12**, **13**)^{114,122,123} and its thiol analogue, 2-mercaptoglutarate (2MG, **14**),¹²⁴ have also been shown to inhibit AlkB demethylases (Table 3). The crystal structure of 2HG bound to AlkB demethylases has not been determined to date, nevertheless the structures of *R*-2HG **12** and *S*-2HG **13** bound to FIH and KDM4A have been solved (PDB ID_{FIH}: 2YC0 & 2YDE; PDB ID_{KDM4A}: 2YBK & 2YBS),¹²³ showing a similar mode of binding as 2OG. In particular, 2HG coordinates to iron in a bidentate manner through its C-1 carboxylate oxygen and C-2 hydroxyl group, whilst its C-5 carboxylate is positioned to hydrogen bond to the conserved asparagine residue.

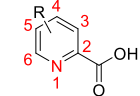
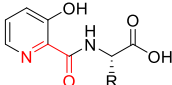
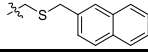
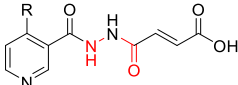
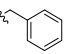
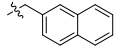
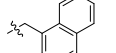
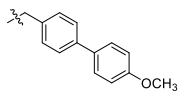
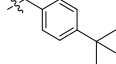
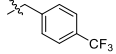
Although these endogenous metabolites only weakly inhibit AlkB demethylases and other Fe(II)/2OG-oxygenases, accumulation of these metabolites above physiological 2OG levels (> 10 mM), as observed with certain mutations of TCA cycle genes, can cause significant inhibition of these enzymes, which can lead to cancers.^{116,121-125} Of particular interest are gain-of-function mutations in two isoforms of isocitrate dehydrogenases, IDH1 and IDH2, which are strongly associated with acute myeloid leukaemia and gliomas.¹²¹⁻¹²⁵ These mutations replace the normal catalytic functions of IDH1 and IDH2 (*i.e.* decarboxylation of isocitrate to 2OG)

with a new function (*i.e.* reduction of 2OG to *R*-2HG), consequently causing a marked elevation of 2HG levels coupled with a depletion of 2OG. The precise pathway leading to cancer is not clear. It has been proposed that elevated levels of 2HG may alter the epigenetic gene regulatory functions of AlkB demethylases and JmjC KDMs that promote tumorigenesis. Alternatively, it could inhibit DNA repair by ALKBH2 and ALKBH3, leading to genetic mutations and progression of tumours.¹²⁵ In recent years, it is also clear that some cancers, such as renal cell carcinomas and paragangliomas are caused by mutations in succinate dehydrogenase (SDH) and fumarate hydratase (FH) which gives rise to abnormally high levels of succinate and fumarate, respectively.¹²⁵

Pyridine dicarboxylate analogues. 2,4-Pyridine dicarboxylic acid (2,4-PDCA **15**) is a cyclic analogue of 2OG. As with NOG, it is a well-established, broad spectrum inhibitor of AlkB demethylases and other Fe(II)/2OG-oxygenases (Table 4).¹²⁶⁻¹²⁸ Crystallographic analyses of **15** bound to FTO (PDB ID: 4IE0)¹¹⁴ and ALKBH5 (PDB ID: 4NRQ)³⁸ revealed that **15** chelates to active site iron *via* its pyridyl nitrogen and C-2 carboxylate oxygen in a bidentate manner. The C-4 carboxylate group of **15** further forms two salt-bridges interactions with a conserved Arg residue and a hydrogen-bond with the side chains of Tyr residue. These additional interactions are crucial for inhibitory activity, as evidenced by a dramatic loss of potency of isomers **16** (2,5-PDCA) and **18** (2,3-PDCA), where the corresponding carboxylate groups are unable to participate in equivalent interactions with the Arg and Tyr residues (Table 4).¹²⁷

3-Hydroxypyridine carboxamide analogues. Following the discovery of 2,4-PDCA, several analogues have been developed through a combination of high-throughput screening, structure-based design and computational approaches. One notable class is the 3-hydroxypyridine carboxamides (Table 4). A number of compounds from this class *i.e.* **19-21** showed good activity against AlkB, with IC₅₀ values ranging from 3.4 μM to 9.5 μM,¹¹² which is at least 9-fold more potent compared to 2,4-PDCA (IC₅₀ = 84 μM).¹²⁷ Their potency is apparently due to the presence of a 3-hydroxyl group, which enables strong hydrogen-bonding interactions with the side chain of Ser145 in AlkB. A crystal structure of AlkB in complex with **19** (PDB ID: 3T3Y)¹¹² reveals that **19** binds differently to the manner observed for 2,4-PDCA and NOG (Figure 3B). Specifically, the pyridine ring of **19**, instead of occupying the metal-binding site, ‘flips over’ to occupy a neighbouring hydrophobic pocket buried within the core of the jelly-roll fold, so as to enable π-π interactions with the side chain of Trp178 (Figure 3B). Consequently, the pyridyl nitrogen of **19** is shifted *trans* to the proximal His131 (rather than *trans* to Asp133) whilst the C-1 carboxylate oxygen is *trans* to Asp133 (rather than *trans* to distal His187). Interestingly, this unique mode of binding appears to be specific for AlkB, as it is not observed in the structures of **19** bound to FTO (PDB ID: 4IE5),¹¹⁴ FIH (PDB ID: 2W0X),¹¹⁰ and KDM4A (PDB ID: 2VD7).¹²⁸ In these complexes, the pyridine ring of **19** is positioned within the 2OG metal-binding site where it participates in bidentate metal chelation.

Table 4. Available inhibition data for pyridine dicarboxylate analogues, 3-hydroxypyridine carboxamide analogues and acylhydrazine analogues against AlkB demethylases and other Fe(II)/2OG-dependent oxygenases. The metal chelating motif is highlighted in red. Horizontal lines indicate no inhibition data are available.

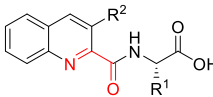
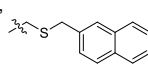
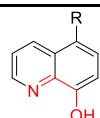
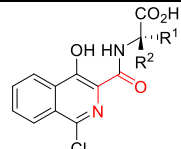
Code	IC ₅₀ /μM					Other Fe(II)/2OG-oxygenases	Structures
	AlkB	FTO	ALKBH2	ALKBH3	ALKBH5		
15	84 ¹²⁷	–	–	–	9.43 ⁸²	FIH (1.1) ¹²⁶ PHD2 (6) ¹²⁶ KDM2A (4.1) ¹²⁶ KDM4E (4.7) ¹²⁸ PHF8 (153) ¹²⁶ BBOX1 (82) ¹²⁸	
16	193 ¹²⁷	–	–	–	–	KDM4E (1900) ¹²⁸	15 2,4-PDCA R ⁴ = CO ₂ H
17	64 ¹²⁷	–	–	–	–	KDM4E (250) ¹²⁸	16 2,5-PDCA R ⁵ = CO ₂ H
18	479 ¹²⁷	–	–	–	–	KDM4E (>10000) ¹²⁸	17 2,6-PDCA R ⁶ = CO ₂ H 18 2,3-PDCA R ³ = CO ₂ H
19	3.4 ¹¹²	15 ¹¹⁴	–	–	–	PHD2 (409) ¹⁰³ FIH (91.09) ¹¹⁰	
20	9.5 ¹¹²	–	–	–	–	–	19 R = H 20 R = CH ₃
21	7.9 ¹¹²	92 ¹¹⁴	–	–	–	–	21 R = 
22	168.8 ¹⁰⁶	11.8 ¹⁰⁶	152.3 ¹⁰⁶	114.6 ¹⁰⁶	167.9 ¹⁰⁶	–	
23	33.5 ¹⁰⁶	0.81 ¹⁰⁶	25.9 ¹⁰⁶	66.2 ¹⁰⁶	108.1 ¹⁰⁶	PHD2 (>100) ¹⁰⁶ KDM4A (>300) ¹⁰⁶	22 R = H 23 LipotF R = 
24	–	1.70 ¹⁰⁶	–	–	–	–	24 R = 
25	–	1.48 ¹⁰⁶	–	–	–	–	25 R = 
26	–	1.28 ¹⁰⁶	–	–	–	–	26 R = 
27	–	2.11 ¹⁰⁶	–	–	–	–	27 R = 
28	–	3.05 ¹⁰⁶	–	–	–	–	28 R = 

Superposition of AlkB-**19** complex with FTO-**19** complex indicates that the hydrophobic pocket (in which the pyridine ring of **19** binds in AlkB) is too small in FTO to accommodate the pyridine ring; this likely accounts for, at least in part, the different binding mode of **19** in AlkB and FTO.¹¹⁴

Acylhydrazine derivatives. Another class of inhibitors of interest is the acylhydrazine derivatives **22–28** (Table 4),¹⁰⁶ which are in fact acyclic mimics of 2,4-PDCA. These inhibitors are unique in that they contain two binding motifs which allow them to occupy the 2OG-binding site and nucleotide-binding site concurrently, thus inhibiting the binding of both co-substrate and substrate (Figure 3C). In particular, each inhibitor contains a 2OG-binding motif which comprises of a fumarate hydrazine moiety. It chelates to the active site iron *via* the hydrazine nitrogen and C-2 carboxylate, thus anchoring the molecule strongly into the 2OG-binding site. Each inhibitor also contains a substrate-binding motif which usually consists of an appropriately substituted pyridine side chain. This motif inserts into

the substrate binding site and mimics the binding of N³-methylthymidine (m³T) substrate to FTO. m³T was selected as a model for nucleotide binding because it is apparently an exclusive substrate of FTO, not significantly demethylated by other AlkB subfamily members. Presumably differences in residues lining in the nucleotide-binding sites of the AlkB subfamilies allow m³T to bind more strongly, and thus preferentially, to FTO compared to other AlkB subfamily members. Hence, by simulating the unique interactions of m³T, the pyridine side chain confers selectivity towards FTO. This design strategy led to the discovery of a series of highly potent and selective FTO inhibitors **22–28** (Table 4).¹⁰⁶ LipotF **23** (IC₅₀ = 0.81 μM),¹⁰⁶ in particular, is the first inhibitor to demonstrate subfamily-selectivity for FTO- it is 30-fold to 130-fold more selective for FTO over other AlkB subfamilies, and >100-fold selective against PHD2 and KDM4A (Table 4).¹⁰⁶ Moreover, the cell-penetrating ethyl ester prodrug of **23** is able to inhibit m⁶A demethylase activity in cells, thus compound **23** is likely useful as

Table 5. Available inhibition data for quinoline and isoquinoline carboxamide derivatives against AlkB demethylases and other Fe(II)/2OG-dependent oxygenases. The metal chelating motif is highlighted in red. Values in % refer to percentage inhibition at a final concentration of 100 μ M. Horizontal lines indicate no inhibition data are available.

Code	IC ₅₀ / μ M					Other Fe(II)/2OG-oxygenases	Structures
	AlkB	FTO	ALKBH2	ALKBH3	ALKBH5		
29	165 ¹¹²	–	–	–	–	–	 <p>29 R¹ = H, R² = H 30 R¹ = H, R² = OH 31 R¹ = H, R² = </p>
30	42.5 ¹¹²	–	–	–	–	–	
31	22.3 ¹¹²	–	–	–	–	–	
32	10.2 ¹²⁶	3.3 ¹¹⁴	–	–	2.9 ¹²⁹	FIH (20) ¹³⁰ PHD2 (15) ¹³⁰ KDM4A (4.8) ¹³¹	 <p>32 IOX1 R = CO₂H 33 R = SO₂NH₂ 34 R = SO₂NHCH₃</p>
33	–	23 ¹¹⁴	–	–	–	–	–
34	–	18 ¹¹⁴	–	–	–	–	–
35	–	2.8 ¹¹⁴	–	–	39.8% ⁸²	FIH (>25) ¹³⁰ PHD2 (0.07) ¹³⁰	 <p>35 IOX3 R¹ = H, R² = H 36 (D-) R¹ = H, R² = CH₂C₆H₅ 37 (L-) R¹ = CH₂C₆H₅, R² = H 38 (D-) R¹ = H, R² = CH₃ 39 (L-) R¹ = CH₃, R² = H 40 (D-) R¹ = H, R² = CH(CH₃)₂ 41 (L-) R¹ = CH(CH₃)₂, R² = H</p>
36	–	38 ¹¹⁴	–	–	–	–	–
37	–	84 ¹¹⁴	–	–	–	–	–
38	–	60 ¹¹⁴	–	–	–	–	–
39	–	110 ¹¹⁴	–	–	–	–	–
40	–	120 ¹¹⁴	–	–	–	–	–
41	–	160 ¹¹⁴	–	–	–	–	–

functional probe to interrogate the epigenetic mechanism of FTO.¹⁰⁶

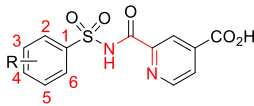
Crystallographic and structural alignment studies (PDB ID of FTO-**23** complex: 4CXW)¹⁰⁶ suggest that the selectivity of **23** is likely attributed to two important interactions with the nucleotide-binding site of FTO, namely 1) π - π stacking interaction between the pyridine ring of **23** and the side chains of Tyr108 and His231, and 2) a hydrogen-bonding interaction between pyridyl nitrogen and amide backbone of Glu234 (Figure 3C).¹⁰⁶ Equivalent interactions between **23** and other AlkB subfamilies are either prohibited or insignificant, hence rationalising, at least in part, the specificity of **23** towards FTO. Interestingly, analogues of **23** bearing various substituted benzyl and naphthalene side chains *i.e.* **24-28** also display good potency against FTO, with IC₅₀ values in the low micromolar range (1-3 μ M).¹⁰⁶ This suggests that the nucleotide-binding site is likely conformationally-flexible and provides opportunities to further improve the potency and selectivity of this class of inhibitors. This ‘dual warheads’ strategy could potentially be exploited for the selective inhibition of other AlkB subfamilies and other Fe(II)/2OG-dependent oxygenases.

Quinoline and isoquinoline carboxamide derivatives.

Recently, a number of heterocyclic compounds carrying the quinoline carboxamide (**29-34**) or isoquinoline-3-carboxamide (**35-41**) scaffolds have been reported as AlkB demethylase inhibitors (Table 5). These compounds were discovered through various approaches, including DCMS

techniques, high-throughput screening and structure-based design.^{112,114,126} Of particular interest are IOX1 **32** and IOX3 **35**, which are cell-active broad spectrum inhibitors, with demonstrated activities against *E. coli* AlkB, FTO, ALKBH5 and other Fe(II)/2OG-oxygenases, including FIH, PHD2 and KDM4A.^{82,112,114,126,129-131} IOX1 **32** was initially developed as a PHD2 inhibitor; it has been shown to stabilise HIF-1 α in a variety of human cell lines, including renal carcinoma (RCC4), embryonic kidney (293T) and bone osteosarcoma (U2OS), thus **32** is widely used to induce pseudo-hypoxia in functional studies.^{126,132} The crystal structures of **32** bound to AlkB (PDB ID: 4JHT)¹²⁶ and FTO (PDB ID: 4IE4)¹¹⁴ have been reported. In both complexes, **32** is observed to coordinate to active site metal *via* the quinolyl nitrogen atom and the oxygen atom in the adjacent hydroxyl group, however **32** adopts different binding orientations in AlkB and FTO. With FTO, **32** binds in an analogous manner as 2,4-PDCA **15**, where the quinolyl nitrogen is positioned *trans* to aspartate (Asp233) and the hydroxyl oxygen *trans* to the distal histidine (His307).¹¹⁴ The C-5 carboxylate group of **32** is also positioned similarly to that observed for the 4-carboxylate group of 2,4-PDCA to participate in two salt bridge interactions with the conserved arginine (Arg316). With AlkB, however, the metal coordination positions of **32** are switched, such that the quinolyl nitrogen is situated *trans* to the proximal histidine (His131) whilst the hydroxyl oxygen is *trans* to the aspartate (Asp133).¹²⁶ Furthermore, the C-5 carboxylate of **32** is shifted to a slightly different position

Table 6. Available inhibition data for pyridine sulfonamide derivatives against AlkB demethylases. The metal chelating motif is highlighted in red. Horizontal lines indicate no inhibition data are available.

Code	IC ₅₀ /μM					Structures
	AlkB	FTO	ALKBH2	ALKBH3	ALKBH5	
42	–	26.4 ¹³⁶	65.2 ¹³⁶	>500 ¹³⁶	>500 ¹³⁶	 <p>42 R = H 43 R⁴ = CF₃ 44 R² = CH₃ 45 R³ = CH₃ 46 R⁴ = CH₃ 47 R², R⁵ = CH₃ 48 R², R⁴ = CH₃ 49 R², R⁴, R⁶ = CH₃ 50 R² = CF₃ 51 R² = NO₂</p>
43	–	2.6 ¹³⁶	42.7 ¹³⁶	69.1 ¹³⁶	201.3 ¹³⁶	
44	–	105.6 ¹³⁶	56.4 ¹³⁶	3.7 ¹³⁶	128.2 ¹³⁶	
45	–	5.8 ¹³⁶	56.6 ¹³⁶	11.4 ¹³⁶	>300 ¹³⁶	
46	–	4.6 ¹³⁶	25.8 ¹³⁶	23.3 ¹³⁶	75.5 ¹³⁶	
47	–	4.0 ¹³⁶	10.8 ¹³⁶	25.1 ¹³⁶	>300 ¹³⁶	
48	–	7.9 ¹³⁶	85.3 ¹³⁶	41.3 ¹³⁶	68.4 ¹³⁶	
49	–	5.2 ¹³⁶	106.9 ¹³⁶	21.2 ¹³⁶	>300 ¹³⁶	
50	–	36.7 ¹³⁶	46.2 ¹³⁶	22.5 ¹³⁶	>300 ¹³⁶	
51	–	9.5 ¹³⁶	13.8 ¹³⁶	6.2 ¹³⁶	1.8 ¹³⁶	

such that only one of its carboxylate oxygens is able to interact with the conserved arginine residue (Arg204). Presumably, **32** is forced into this ‘constrained’ binding orientation due to steric clash with several residues in the 2OG-binding site of AlkB (e.g. Asn120, Tyr122 and Leu128). This apparently weaker binding mode likely accounts for the reduced potency of **32** for AlkB (IC₅₀ = 10.2 μM) compared to FTO (IC₅₀ = 3.3 μM; Table 5).^{114,126}

IOX3 **35**, also known as FG-2216, is a potent (IC₅₀ = 3.9 μM) and orally-active PHD2 inhibitor developed by Fibrogen for the treatment of anaemia.^{130,133} Results from clinical trials showed that **35** significantly increased the levels of haemoglobin in patients by inducing erythropoietin production.^{134,135} Several stereoisomeric analogues of **35** have been reported (compounds **36-41**; Table 5). Structure-activity studies found that substitution at the C-α position of **35** generally reduces potency towards FTO. Furthermore, FTO appears to favour the *D*-enantiomers (**36, 38, 40**) over the *L*-enantiomers (**37, 39, 41**).¹¹⁴ This contrasts with AlkB, where the *L*-isomers are preferred (Compounds **2-6**; Table 3). Thus, manipulation of stereoisomeric substitutions in these scaffolds may drive selectivity towards a particular AlkB subfamilies.

Crystallographic analysis revealed that **35** binds to FTO in a similar manner to that observed for 3-hydroxypyridine carboxamides **19**, although the exact orientation and metal coordination positions of **35** and **19** differ slightly (PDB ID of FTO-**35** complex: 4IE6; for binding of **19** to FTO, see Section on ‘3-hydroxypyridine carboxamides’).^{112,114} In particular, the relatively large isoquinoline ring of **35** was twisted out of plane with respect to the carboxamide side chain by ~60°, apparently to avoid steric clash with the conserved Arg96 residue (Figure 3D). As a result of the change in conformation, the coordination of isoquinoline nitrogen to the active site metal is also skewed. Despite the ‘non-ideal’ binding geometry, compound **35** (IC₅₀ 2.8 μM) has similar potency as **32** towards FTO (IC₅₀ 3.3 μM; Table 5).¹¹⁴ Interestingly, the chlorine atom of **35** was observed to project into the substrate-binding site of FTO.

Recently, a crystal structure of ALKBH5 in complex with **35** (PDB ID: 4NJ4)⁸² has been solved which showed **35**

binding away from the 2OG-binding pocket, where it forms a covalent link to the side chain of Cys200 with the loss of a chlorine atom. As noted by the authors,⁸² the observed *S*-arylation reaction likely occurred as a result of prolonged crystallisation process (of up to 12 weeks) and is likely not relevant to the inhibition of ALKBH5. Nevertheless, the propensity for **35** to participate in alkylation reaction with cysteine does raise the question about safety of **35** and, more generally, other C-1 chlorinated isoquinoline derivatives in clinical application. Further studies to clarify the inhibition mechanism and toxicity profile of this class of inhibitors are needed.

Pyridine sulphonamide derivatives. More recently, a new class of AlkB demethylase inhibitors based on the pyridine sulphonamide scaffolds **42-51** (Table 6) have been identified through a novel approach known as multiprotein dynamic combinatorial chemistry (DCC).¹³⁶ In this strategy, peptide tags of appropriate length were conjugated to the target proteins to modify their melting temperatures, such that their individual melting profiles and that of resulting protein-ligand complexes could be simultaneously monitored in a single differential scanning fluorometric (DSF) melting analysis.¹³⁶ Unlike conventional DCC methods, multiprotein DCC allows several protein templates to be used concurrently in the same dynamic system, thus permitting the discovery of ligands against several proteins simultaneously. Moreover, when structurally-related protein isoforms were used in concert, ligands that are selective for a particular isoform are preferentially assembled and identified. As a proof-of-principle study, the authors applied the multiprotein DCC method to three AlkB subfamily members FTO, ALKBH3 and ALKBH5. This led to the simultaneous discovery of compounds **43** (IC₅₀ = 2.6 μM) and **44** (IC₅₀ = 3.7 μM) as subfamily-selective inhibitors of FTO and ALKBH3, respectively.¹³⁶ Both compounds **43** and **44** showed significantly reduced activity for other AlkB subfamilies (IC₅₀s > 40 μM), and negligible activity against KDM4A (IC₅₀ > 100 μM).¹³⁶ The study further identified **51** as a pan-inhibitor of AlkB demethylases (Table 6).¹³⁶

Structure-activity relationship studies suggest that regiochemistry is likely important in fine-tuning the selectivity of this class of compounds.¹³⁶ For instance, positioning a

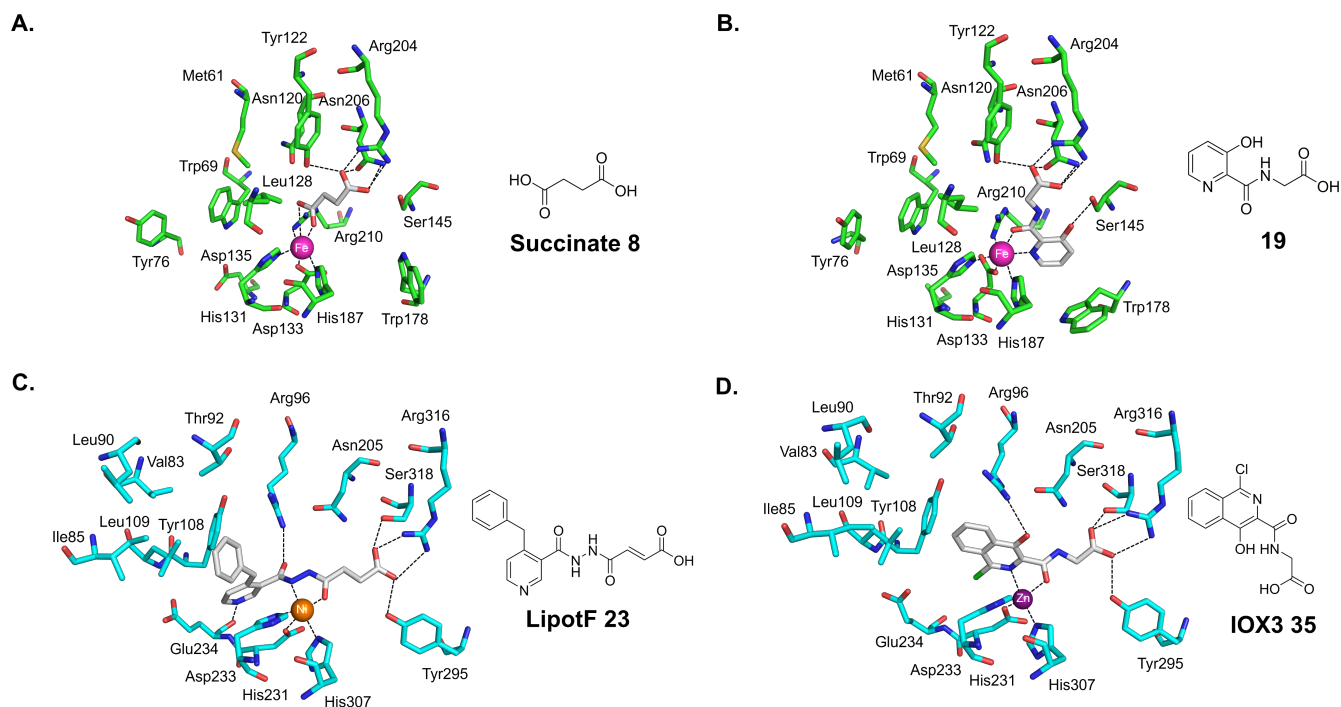


Figure 3. Different modes of binding of inhibitors to the 2OG-binding site of AlkB demethylases. Views of the crystal structures of AlkB (green residues) in complex with (A) succinate **8** (PDB ID: 2FDJ)⁸⁵ and (B) compound **19** (PDB ID: 3T3Y),¹¹² and of FTO (cyan residues) in complex with (C) LipotF **23** (PDB ID: 4CXW)¹⁰⁶ and (D) IOX3 **35** (PDB ID: 4IE6).¹¹⁴ Distinctly different orientations and metal coordination positions were observed for the inhibitors.

methyl group at the 2-position of the phenyl ring directs selectivity towards ALKBH3 (compare **42** with **44**; Table 6), whereas shifting the methyl group to the 3- or 4-positions promotes FTO selectivity (compare **42** with **45** and **46**).¹³⁶ Installing a trifluoromethyl substituent at the 4-position of the phenyl ring (*i.e.* **43**) also favours FTO selectivity whilst moving it to the 2-position (*i.e.* **50**) abolished selectivity.¹³⁶ The presence of two or more methyl groups *i.e.* **47**, **48** and **49** appears to drive selectivity towards FTO. Notably, the position and number of substituents appear to have little or no effect on selectivity towards ALKBH2 and ALKBH5 (Table 6).¹³⁶ Modelling studies suggest that this class of inhibitors likely binds to the 2OG-binding site where it chelates to active site iron through the pyridyl nitrogen and the sulphonamide nitrogen.¹³⁶ The pyridyl carboxylate group likely forms salt bridge interactions with an arginine residue in the conserved R...R motif, whilst the carboxamide carbonyl and sulphonyl oxygens likely participate in hydrogen-bonding interactions with the other conserved arginine residue.¹³⁶ Detailed crystallographic studies are needed to rationalise the selectivity of compounds **43** and **44**, and to provide a structural basis for further optimisation of this class of inhibitors.

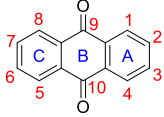
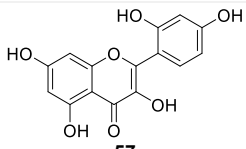
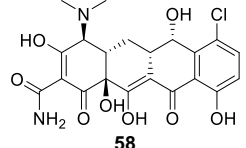
4.2 Inhibitors that bind exclusively to the substrate-binding site

Recent inhibition work on AlkB demethylases is beginning to reveal a new class of inhibitors with a novel mode of

binding, which departs from active-site metal chelation. Compounds in this inhibitor class bind exclusively to the substrate-binding site and, unlike the 2OG-competitive inhibitors which contain a characteristic metal-chelation moiety, they are chemically-diverse and do not possess any specific structural features that easily identifies their mode of binding. These compounds are largely discovered through high-throughput *in silico* and/or biochemical screenings. In this section, the inhibitors were loosely categorised based on their structural scaffold. Tables 7-9 summarise all the available IC₅₀ data and chemical structures of this class of inhibitors.

Rhein and analogues. Rhein **52** is a naturally occurring anthraquinone predominantly found in rhubarb and other plants of the genus *Rheum L* (Table 7).¹³⁷ This natural product is used extensively in traditional Chinese medicine and is known to possess a range of pharmacological activities, including antibacterial, anti-inflammatory, antitumour and antioxidant activities.¹³⁷ Rhein was recently found to be a relatively potent inhibitor of FTO (IC₅₀ = 2.2 – 21 μM)^{138,139} through a series of structure-based virtual screening campaign. This is rather surprising given that rhein does not possess any functional group or binding motif which enables metal chelation. Its mode of binding and inhibition was not clear until a crystal structure of rhein bound to FTO (PDB ID: 4IE7, Figures 4 and 5A) was solved by Aik *et al.*¹¹⁴ The structure revealed that rhein disrupts the binding of

Table 7. Available inhibition data for rhein and analogues against AlkB demethylases. Horizontal lines indicate no inhibition data are available.

Code	IC ₅₀ /μM		Structures
	FTO	Other AlkB demethylases	
52	21.0, ¹³⁸	AlkB (12.7) ¹⁴⁰	 <p>52 Rhein R¹ = OH, R³ = CO₂H, R⁸ = OH 53 R¹ = NH₂, R² = SO₃Na, R⁴ = Br, R⁶ = SO₃Na 54 R¹ = NH₂, R² = SO₃Na, R⁴ = Br 55 R¹ = NHCH₂CH₂NHCH₂CH₂OH R² = NHCH₂CH₂NHCH₂CH₂OH, R⁵ = OH, R⁸ = OH 56 R¹ = OH, R³ = CH₃, R⁶ = OH, R⁸ = OH</p>
	2.18 ¹³⁹	ALKBH2 (9.1) ¹⁴⁰ ALKBH3 (5.3) ¹⁴⁰ ALKBH5 (9.96) ¹³⁹	
53	64.0 ¹³⁹	–	
54	68.0 ¹³⁹	–	
55	1.2 ¹³⁹	–	
56	4.53 ¹³⁹	–	
57	2.58 ¹³⁹	ALKBH5 (7.13) ¹³⁹	 <p>57</p>
58	1.39 ¹³⁹	–	 <p>58</p>

nucleic acid substrate by occupying the substrate-binding site, where it makes three important interactions. First, the carboxylate side chain of rhein is positioned to hydrogen bond with the side chain of Ser229. Second, its C-1 hydroxyl group participates in hydrogen bonding interaction with the side chain of Arg96. Third, the A-ring of rhein is positioned to form π - π interactions with the imidazole ring of the iron-chelating His231 residue. Rhein represents the first example of small molecule inhibitor that binds specifically to the substrate-binding site of FTO. The rhein scaffold therefore provides opportunity for the design of inhibitors that inhibit AlkB subfamilies through substrate competition.

Subsequent biochemical and cell-based analyses found that rhein is cell-permeable, relatively non-cytotoxic and is able to inhibit the m⁶A demethylase activity of FTO in cells.¹³⁸ It exhibits inhibitory activity against several AlkB subfamilies, including AlkB, ALKBH2, ALKBH3 and ALKBH5 (Table 7).^{139,140} Inhibition of the DNA repair function of ALKBH2 and ALKBH3 by rhein, in particular, led to an accumulation of DNA damage, rendering cells susceptible to methylated DNA damage.¹⁴⁰ Rhein also modulates the activity of a broad range of human enzymes, including JmjC KDMs, histone deacetylase (HDAC) classes I/II and multiple cytochrome P450 (CYP) enzymes. The broad physiological effects of rhein preclude its use as functional probe.

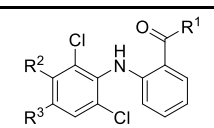
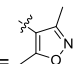
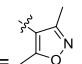
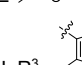
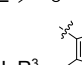
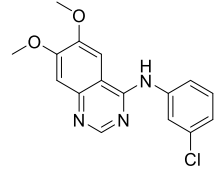
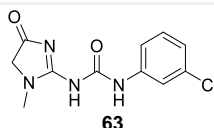
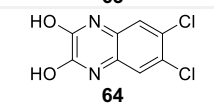
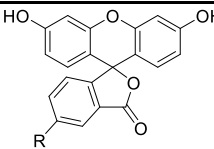
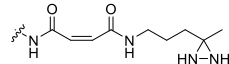
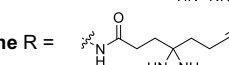
Following these studies, several analogues of rhein carrying the anthraquinone (compounds **53-56**), flavonoid (compound **57**), or tetracycline scaffolds (compound **58**) were identified as potent inhibitors of FTO through a novel high-throughput screening approach that uses fluorometric RNA aptamer substrates.¹³⁹ The exact mode of binding for

these analogues is unknown at present, nevertheless, given their close structural similarity to rhein, they likely occupy the substrate-binding site, in a manner similar to rhein.

Meclofenamic acid and analogues. Recent high-throughput screening of a library of 900 randomly selected drugs using a fluorescence polarisation assay led to the identification of meclofenamic acid (MA) **59** as a substrate-competitive inhibitor of FTO (Table 8).^{139,141} Meclofenamic acid is a derivative of anthranilic acid, non-steroidal anti-inflammatory drug, approved by the FDA for the treatment of dysmenorrhoea, joint pain, muscular pain and arthritis.¹⁴² It prevents the formation of prostaglandins *via* inhibition of cyclooxygenase (COX) enzyme, however, due to a high rate (30-60%) of gastrointestinal side effects, this drug is not widely used in humans.

Crystallographic studies of FTO in complex with meclofenamic acid **59** and NOG **1** (PDB ID: 4QKN; Figure 5B)¹⁴¹ by Yang *et al.* revealed that meclofenamic acid, as with rhein, occupies the substrate-binding site of FTO, thus obstructing the access of nucleic acid substrate (Figures 4 and 5B). Binding of meclofenamic acid to FTO is achieved through a number of key interactions. First, the carboxylate group of meclofenamic acid forms two hydrogen bonding interactions – one with the amide backbone of Ser229 and the other with the amide backbone of Lys216 *via* a water molecule. Second, the phenyl ring (on which the carboxylate group is attached) further participates in hydrophobic interactions with the side chains of neighbouring Ile85, Leu90 and Pro93 residues. Third, one of the chlorine atoms is also positioned to form polar interactions with the side chain of Arg96. Crucially, meclofenamic acid interacts with parts of the first loop in the nucleotide recognition lid of FTO

Table 8. Available inhibition data for meclofenamic acid and fluorescein analogues against AlkB demethylases. Horizontal lines indicate no inhibition data are available.

Code	IC ₅₀ / μM		Structures
	FTO	Other AlkB demethylases	
59	8.0, ¹⁴¹ 7.94 ¹³⁹	ALKBH2/3 (>100) ¹⁴¹ ALKBH5 (>100), ¹⁴¹ (>20) ¹³⁹	 <p>59 MA R¹ = OH, R² = CH₃, R³ = H</p>
60	0.06 ¹⁰⁷	–	
61	2.6 ¹⁰⁷	–	 <p>60 FB23 R¹ = OH, R² = H, R³ = </p>  <p>61 FB23-2 R¹ = NHOH, R² = H, R³ = </p>
62	3.0 ¹³⁹	–	 <p>62</p>
63	3.31 ¹³⁹	–	 <p>63</p>
64	4.97 ¹³⁹	–	 <p>64</p>
65	3.23 ¹⁴³	ALKBH5 (>100) ¹⁴³	 <p>65 Fluorescein R = H 66 Fluorescein 2Na⁺ R = H 67 R = NH₂ 68 R = NHCOC₂H₂COOH 69 R = SCN 70 R = NHCOCHCH₂ 71 R = NHCOCH₃ 72 R = NHCOC₆H₅</p> <p>73 68-DZ R =  74 67-DZ-alkyne R = </p>
66	3.65 ¹⁴³	–	
67	6.55 ¹⁴³	–	
68	1.72 ¹⁴³	–	
69	4.12 ¹⁴³	–	
70	4.84 ¹⁴³	–	
71	6.60 ¹⁴³	–	
72	6.65 ¹⁴³	–	
73	4.49 ¹⁴³	–	
74	2.24 ¹⁴³	–	

(formed by β3 and β4), which significantly strengthened its interaction with FTO. This portion of the loop is apparently absent in ALKBH5, rationalising the marked selectivity of meclofenamic acid for FTO (IC₅₀ = 8.0 μM) over ALKBH5 (IC₅₀ > 100 μM).¹⁴¹ Although similar loop structures are present in the nucleotide recognition lid of ALKBH2 and ALKBH3, steric clash with a number of residues in this region (*i.e.* Arg110 in ALKBH2; Arg122, Tyr127 and Asp189 in ALKBH3) prevents the binding of meclofenamic acid to both enzymes and, hence, its poor activity against them (IC₅₀ > 100 μM).¹⁴¹ Results from this study suggests that it is possible

to achieve FTO subfamily selectivity by exploiting interactions with the residues in the nucleotide recognition lid.

The unique mode of binding of meclofenamic acid inspired subsequent structure-based design by the same group, which led to the development of two highly potent and selective FTO inhibitors FB23 **60** and FB23-2 **61** (Table 8).¹⁰⁷ Compound **60** is an analogue of meclofenamic acid wherein an isoxazole ring is appended to the dichlorobenzene moiety. A crystal structure of **60** bound to FTO (PDB ID: 6AKW)¹⁰⁷ reveals a similar mode of binding as meclofenamic acid, with all key interactions conserved. The introduction of an isoxazole ring not only allows an extension of

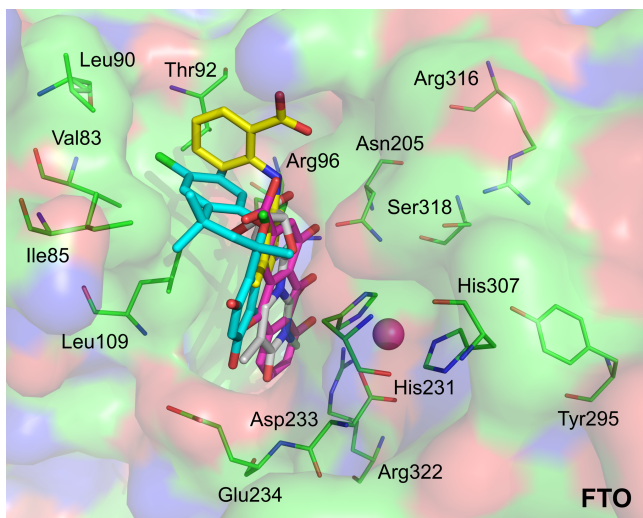


Figure 4. Superposition of the crystal structures of FTO (green) in complex with CHTB (cyan), meclofenamic acid (yellow), rhein (magenta) and m^3T (grey). The three inhibitors occupy a similar region of the substrate-binding site where the nucleotide substrate m^3T binds. The magenta sphere represents the active site metal ion. PDB IDs: CHTB **85** (5F8P), meclofenamic acid **59** (4QKN),¹⁴¹ rhein **52** (4IE7),¹¹⁴ m^3T (3LFM).⁸⁶

the molecule deep into the nucleotide-binding site but, importantly, enables hydrogen bonding interaction with the amide backbone of Glu234; notably, this residue was previously identified to confer selectivity for FTO over other subfamily members (see Section on ‘acylhydrazine derivatives’).¹⁰⁶ As a result of this structural modification, **60** showed a remarkable 130-fold improvement in potency for FTO ($IC_{50} = 0.06 \mu M$) compared to meclofenamic acid ($IC_{50} = 8.0 \mu M$), whilst retaining FTO subfamily selectivity.^{107,141} To improve the cell penetration of compound **60**, the carboxylate group was replaced with a hydroxamate group. This led to analogue **61** which exhibits significantly improved cell permeability.¹⁰⁷ Cell-based studies demonstrated that FTO inhibition by **61** dramatically suppresses proliferation and promotes the differentiation of human acute myeloid leukaemia (AML) cells.¹⁰⁷ Moreover, in patient-derived AML mouse models, **61** significantly inhibits the progression of AML cells and prolongs survival of the animal,¹⁰⁷ suggesting that FTO inhibition could be a promising strategy for the treatment of AML.

Fluorescein and derivatives. Following the discovery of meclofenamic acid, Zhou *et al.*¹⁴³ screened a library of fluorescent molecules that are structurally-related to meclofenamic acid, with a view to developing fluorescent FTO inhibitors that not only modulate the demethylase activity of FTO, but also enable direct photoaffinity labelling of FTO in cells. The group found, rather unexpectedly, that fluorescein **65** and some of its derivatives *i.e.* compounds **66-74** can selectively inhibit FTO demethylation with IC_{50} values in the low micromolar range; the most potent inhibitor being **68** ($IC_{50} = 1.72 \mu M$; Table 8).¹⁴³ The inhibitors displayed high selectivity towards FTO over ALKBH5. Compounds **70** and

Table 9. Available inhibition data for benzene-1,3-diols and entacapone analogues against AlkB demethylases. Values in % refer to percentage inhibition at a final concentration of 100 μM ; horizontal lines indicate no inhibition data are available. Inhibition data for other AlkB demethylases are not available.

Code	$IC_{50}/\mu M$	Structures
	FTO	
75	4.95 ¹⁴⁴	<p>75 CDPCB R = H 76 R² = F, R⁶ = F 77 R² = Cl, R⁶ = Cl 78 R³ = Cl 79 R² = Cl 80 R³ = OC₆H₅ 81 R⁴ = OH 82 R³ = (CH₂)₃CH₃ 83 R³ = Br</p>
76	15.2% ¹⁴⁴	
77	15.4% ¹⁴⁴	
78	16.9% ¹⁴⁴	
79	16.9% ¹⁴⁴	
80	17.3% ¹⁴⁴	
81	17.8% ¹⁴⁴	
82	18.2% ¹⁴⁴	
83	18.7% ¹⁴⁴	
84	18.4% ¹⁴⁴	
85	39.24 ¹⁴⁵	<p>85 CHTB</p>
86	16.04 ¹⁴⁶	<p>86 Radicol</p>
87	3.5 ¹⁴⁷	<p>87 Entacapone R¹ = H, R² = N(C₂H₅)₂ 88 R¹ = OH, R² = N(C₂H₅)₂ 89 R¹ = OH, R² = 90 R¹ = H, R² = 91 R¹ = H, R² = </p>
88	0.5 ¹⁴⁷	
89	0.75 ¹⁴⁷	
90	1.2 ¹⁴⁷	
91	0.7 ¹⁴⁷	

71, which possess better cell permeability were subsequently tested in HeLa cell and found to efficiently inhibit FTO m^6A demethylation at 50 μM .¹⁴³

Crystal structures of FTO-fluorescein **65** complex (PDB ID: 4ZS2; Figure 5C)¹⁴³ and FTO-5-aminofluorescein **67** complex (PDB ID: 4ZS3)¹⁴³ revealed that both inhibitors bind to the substrate-binding site of FTO, in a manner similar to meclofenamic acid. Interestingly, in these co-crystal complexes, the lactone rings of **65** and **67** were hydrolysed

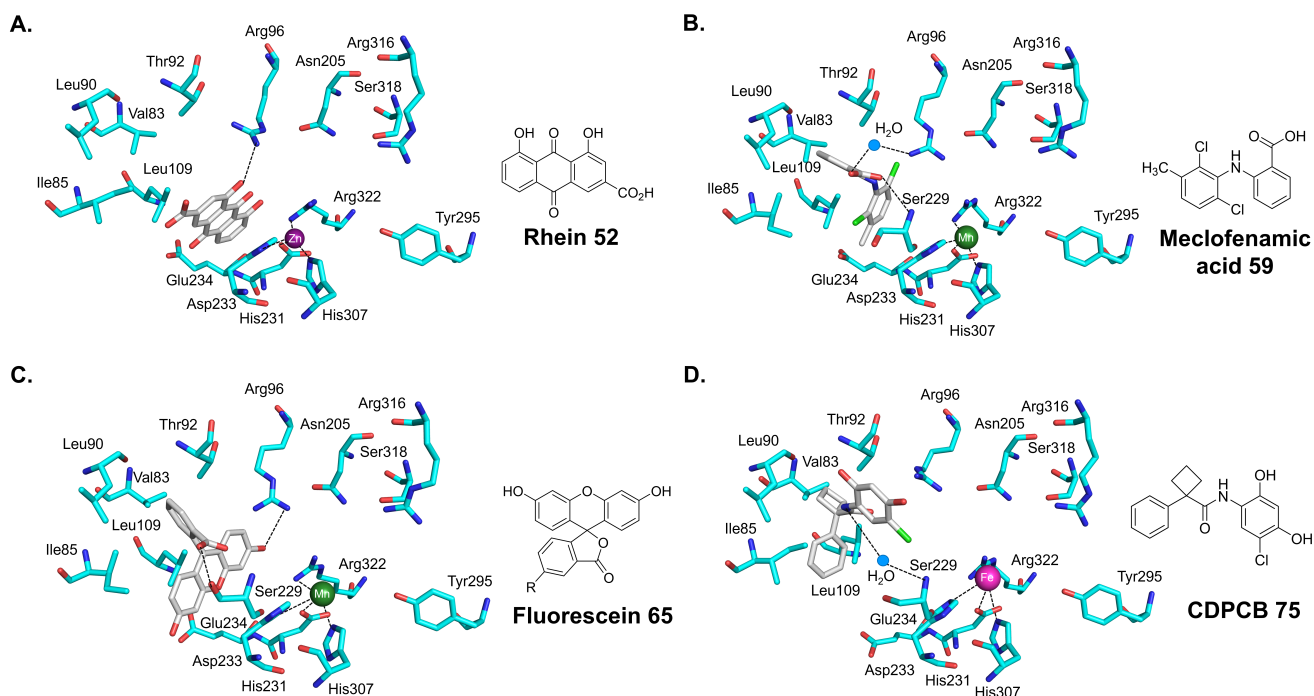


Figure 5. Different modes of binding of inhibitors to the substrate-binding site of FTO. Views of the crystal structures of FTO (cyan residues) in complex with (A) rhein **52** (PDB ID: 4IE7),¹¹⁴ (B) meclofenamic acid **59** (PDB ID: 4QKN),¹⁴¹ (C) fluorescein **65** (PDB ID: 4ZS2),¹⁴³ and (D) CDPCB **75** (PDB ID: 5DAB).¹⁴⁴ Fluorescein and CDPCB adopt different binding orientations and occupy different regions of the substrate-binding site as rhein and meclofenamic acid. For clarity, ligands that bind to the 2OG-binding sites *i.e.* citrate and NOG in Figures 5A and 5B, respectively, and 2OG in Figures 5C and 5D.

to carboxylic acids, which form two hydrogen bonds with Ser229. The resulting phenyl ring is stabilised through hydrophobic interactions with surrounding Val83, Ile65, Leu90, Pro93 and Leu109 residues, which constitutes part of the nucleotide recognition lid. Although the 5-amino group of **67** can hydrogen-bond with the amide backbone of Leu91, this interaction is unfavourable due to clashes with surrounding hydrophobic residues, thus rationalising the weaker inhibitory potency of **67** ($IC_{50} = 6.55 \mu M$) relative to fluorescein **65** ($IC_{50} = 3.23 \mu M$).¹⁴³ Compounds **67** and **68** were subsequently modified to incorporate a photoreactive diazine ring (DZ) to yield **68-DZ** (**73**) and **67-DZ-alkyne** (**74**), which enable photoaffinity labelling and enrichment of cellular FTO.¹⁴³

Benzene,1,3-diol derivatives. To develop novel inhibitor scaffolds that specifically target the substrate-binding site of FTO, Chang *et al.*¹⁴⁴ designed a series of benzene-1,3-diol derivatives **75-86** which mimic the binding of FTO substrate m^3T , of which the most potent inhibitor is CDPCB **75** ($IC_{50} 4.95 \mu M$; Table 9). The activity of **75** against other AlkB demethylases is undetermined at present. Cell-based experiments showed that **75** is relatively non-cytotoxic with good cell-penetration.^{144,145} Treatment of FTO-overexpressing 3T3-L1 preadipocytes with $10 \mu M$ **75** significant increases the levels of m^6A in mRNA.¹⁴⁵ A crystal structure of **75** bound to FTO (PDB ID: 5DAB, Figure 5D)¹⁴⁴

was solved, showing **75** adopting a rather interesting mode of binding which is strikingly different from those observed for the m^3T substrate (PDB ID: 3LFM),⁸⁶ rhein **52** (PDB ID: 4IE7)¹¹⁴ and meclofenamic acid **59** (PDB ID: 4QKN).¹⁴¹ As shown in Figure 5, **75** occupies a region in the substrate-binding site that is closer to the outer solvent-exposed groove of FTO and binds in such a way that it is perpendicular to the orientation of m^3T , rhein and meclofenamic acid, almost blocking the groove entrance. Accordingly, **75** is able to make novel contacts with a number of residues in the antiparallel β -sheet of FTO that was not previously explored. In particular, the cyclobutene ring of **75** forms hydrophobic interactions with the side chains of Leu90 and Thr92, and the amide backbone of Leu91, whereas the unsubstituted phenyl ring interacts with the side chains of Ile85 and Leu109. The binding of **75** is further stabilised by several major interactions between the phenolic ring of **75** and the L1 loop of the nucleotide recognition lid of FTO. Specifically, the C-4 hydroxyl group participates in hydrogen-bonding interactions with the amide backbone of Lys216 and Met226, and the chlorine atom makes van der Waals contacts with Met226, Ala227 and Ser229. The carbonyl oxygen of **75** further forms two water-mediated hydrogen-bonds with the side chain and amide backbone of Ser229.

Following the discovery of **75**, the same group identified another FTO inhibitor, CHTB **85** that similarly carries a benzene-1,3-diol scaffold and binds exclusively to the substrate-binding site ($IC_{50} = 39.24 \mu M$; Table 9).¹⁴⁵ Surprisingly, despite the structural similarity, compound **85** binds to FTO differently to **75**. Superposition of the crystal structures of FTO in complex with **85** (PDB ID: 5F8P; literature to be published), m^3T substrate (PDB ID: 3LFM),⁸⁶ rhein (PDB ID: 4IE7),¹¹⁴ and meclofenamic acid (PDB ID: 4QKN)¹⁴¹ revealed that **85**, in fact, partially overlaps with m^3T and rhein, and occupies a similar region of the substrate-binding site as meclofenamic acid, sharing several key interactions (Figure 4). Specifically, the dihydroxy benzene ring of **85** is sandwiched between the side chains of two highly-conserved His231 and Leu109 residues to participate in hydrophobic interaction. The C-4 hydroxyl group on the benzene ring further forms two hydrogen-bonds: 1) a water-mediated hydrogen-bond with the amide backbone of Glu234, and 2) a direct hydrogen bond with the amide backbone of His232. The C-5 chlorine atom on the benzene ring makes van der Waals contact with the side chain of Tyr109. Additional stabilisation is provided by the chroman ring of **85**, which is nested in a hydrophobic pocket formed by five residues from the antiparallel β -sheet, *i.e.* Val83, Ile85, Leu90, Thr92 and Leu109. The chroman oxygen and hydroxyl group form a water-mediated hydrogen bond with the side chain of Ser229 and the amide backbone of Val94, respectively. The *gem*-dimethyl group further participates in van der Waals interactions with the side chain of Ile85. Treatment of FTO-overexpressing 3T3-L1 cells with **85** ($1 \mu M - 5 \mu M$) led to significant increase in m^6A levels in mRNA; **85** is slight toxicity at concentrations above $10 \mu M$.¹⁴⁵

Subsequent work by the group found that radicicol **86**, a macrocyclic natural product found in the fungus of *Monoascus bonorden* which contains a 1,3-dihydroxyphenyl group, is able to inhibit FTO activity ($IC_{50} = 16.04 \mu M$; Table 9).¹⁴⁶ Despite the distinctly different chemical structure, molecular modelling studies suggested that radicicol likely occupies the substrate-binding site of FTO, with similar binding poses as compound **75**. **86** exhibits a broad range of biological activities, including antitumour effects through interaction with the heat shock protein 90 and bacterial sensor kinase, hence unlikely to be useful as functional probe. Nevertheless, it allows exploration of unique chemical space and provides inspiration for the design of natural product-based AlkB demethylase inhibitors.

Entacapone and derivatives. The dihydroxy benzene compounds, entacapone and derivatives **87-91**, constitute another interesting class of AlkB demethylase inhibitors (Table 9). Entacapone **87** is an FDA-approved drug for the treatment of Parkinson's disease.¹⁴⁷ It was recently identified as an FTO inhibitor ($IC_{50} = 3.5 \mu M$) through 'structure-based hierarchical screening' of FDA-approved drug database.^{147,148} Representative examples of compounds identified in this screening effort are given in Table 9; only selected inhibitors with IC_{50} values below $10 \mu M$ are shown.¹⁴⁷ Additional analogues of entacapone were reported in a patent by the same group.¹⁴⁹ Biochemical analyses shows that entacapone competes with both m^6A -containing oligonucleotide substrates and 2OG for binding to

FTO. Consistent with these results, a structural complex of FTO with entacapone (PDB ID: 6AK4)¹⁴⁷ revealed that entacapone occupies both the 2OG-binding site and substrate-binding site, in a strikingly similar manner as LipotF **23**- an acylhydrazine FTO inhibitor (Table 4, Figure 3C).¹⁰⁶ In particular, the nitrocatechol ring of entacapone resides in the substrate binding site, where the C-3 hydroxyl forms two hydrogen-bonding interactions with the side chains of Arg322 and Tyr106. The diethylpropanamide moiety of entacapone occupies the 2OG-binding site and chelates to the active site metal in a monodentate fashion *via* the nitrile group. The carbonyl group further hydrogen-bonds with the side chain of Asn205.

Cell-based studies showed that entacapone has negligible inhibitory activity on ALKBH5 and TET1 (ten-eleven translocation 1; an m^5C dioxygenase), and it does not significantly alter the DNA methylation and histone methylation patterns in HepG2 cells.¹⁴⁷ Despite toxicity concerns with acrylonitrile compounds in general, entacapone is relatively non-cytotoxic. Moreover, treatment of diet-induced obese mice with entacapone led to significantly reduce body weight and fasting blood glucose levels.¹⁴⁷ The observed effects were apparently due to an inhibition of m^6A demethylation on forkhead box protein O1 (FOXO1) mRNA, which up-regulates FOXO1 expression and FOXO1-mediated metabolic regulation. Thus, entacapone could be a promising lead for the treatment of metabolic disorders. Subsequent structure-based optimisation of entacapone led to compounds **90** and **91** wherein the flexible diethylpropanamide group was replaced with a rigid alicyclic group. Both analogues showed significantly improved activity with IC_{50} values of $1.2 \mu M$ and $0.7 \mu M$, respectively. A crystal structure of **91** bound to FTO (PDB ID: 6AEJ)¹⁴⁷ revealed a similar mode of binding as entacapone. Compound **91** participates in additional electrostatic interaction between the oxygen of 1,3-tetrahydro oxazine substitution and the side chain of Arg316, which likely accounts for the 5-fold increase in potency of **96** ($IC_{50} = 0.7 \mu M$) relative to entacapone ($IC_{50} = 3.5 \mu M$).¹⁴⁷

4.3 Inhibitors with undetermined mode of binding

In this section we discuss inhibitors of AlkB demethylases with undetermined mode of binding and inhibition. The majority of compounds in this inhibitor class are natural products with a broad range of biological targets and pharmacological activities. Nevertheless, they are highly interesting compounds, from an inhibitor design perspective, because their diverse structures provide fresh inspiration for novel inhibitor scaffolds. Table 10 summarises all the available IC_{50} data and chemical structures of this class of inhibitors.

Amiloride, metizoline and derivatives. Recently, a number of FTO inhibitors, including amiloride compounds **92-94**, metizoline compounds **95-98**, and several others with diverse chemical scaffolds **99-103** were identified through a high high-throughput screening assay that uses the RNA aptamer 'Broccoli' to detect m^6A demethylation by FTO.¹³⁹ Some representative examples are given in Table 10.¹³⁹ A number of the identified inhibitors, such as **93** (IC_{50}

Table 10. Available inhibition data for inhibitors with undetermined mode of binding against AlkB demethylases. Values in % refer to percentage inhibition at a final concentration of 10 μM for compound **104** and 50 μM for compound **113**; horizontal lines indicate no inhibition data are available.

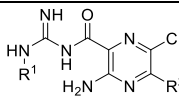
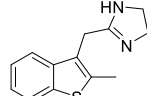
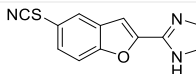
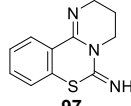
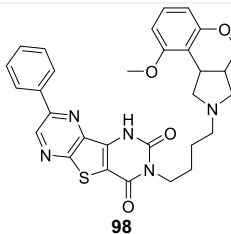
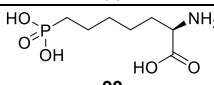
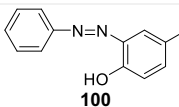
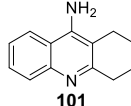
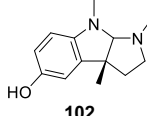
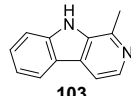
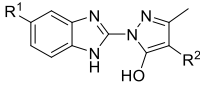
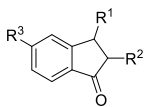
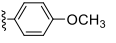
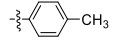
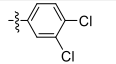
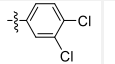
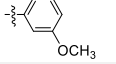
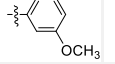
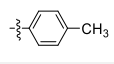
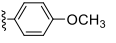
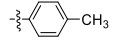
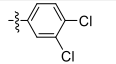
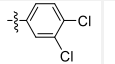
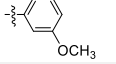
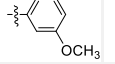
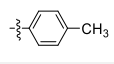
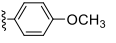
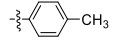
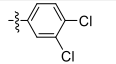
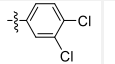
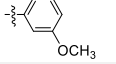
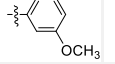
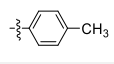
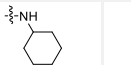
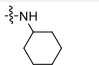
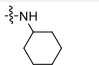
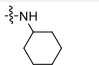
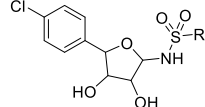
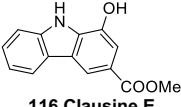
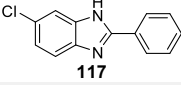
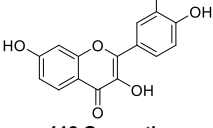
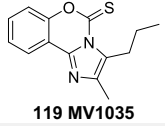
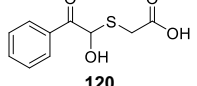
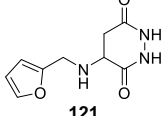
Code	IC ₅₀ / μM			Other AlkB demethylases	Structures
	FTO	ALKBH3	ALKBH5		
92	4.74 ¹³⁹	–	–	–	 <p>92 Amiloride R¹ = H, R² = NH₂ 93 R¹ = H, R² = N(CH₃)₂ 94 R¹ = CH₂C₆H₅, R² = NH₂</p>
93	0.34 ¹³⁹	–	ALKBH5 (1.98) ¹³⁹	–	
94	2.79 ¹³⁹	–	–	–	
95	1.37 ¹³⁹	–	–	–	 <p>95 Metizoline</p>
96	1.62 ¹³⁹	–	–	–	 <p>96</p>
97	2.18 ¹³⁹	–	–	–	 <p>97</p>
98	0.49 ¹³⁹	–	–	–	 <p>98</p>
99	0.85 ¹³⁹	–	ALKBH5 (>20) ¹³⁹	–	 <p>99</p>
100	1.14 ¹³⁹	–	–	–	 <p>100</p>
101	1.71 ¹³⁹	–	–	–	 <p>101</p>
102	1.27 ¹³⁹	–	ALKBH5 (>20) ¹³⁹	–	 <p>102</p>
103	1.23 ¹³⁹	–	ALKBH5 (1.24) ¹³⁹	–	 <p>103</p>

Table 10. continued

Code	IC ₅₀ /μM				Structures																
	FTO	ALKBH3	ALKBH5	Other AlkB demethylases																	
104	–	61% ¹⁵¹	–	–	 <p> 104 R¹ = H, R² = CH₃ 105 HUH5015 R¹ = CH₃, R² = H 106 R¹ = H, R² = CH₂C₆H₅ 107 R¹ = CF₃, R² = CH₂C₆H₅ 108 R¹ = CH₃, R² = 4-Cl benzyl 109 R¹ = F, R² = C₆H₅ </p>																
105	–	0.67 ¹⁵¹	–	–																	
106	–	0.48 ¹⁵¹	–	–																	
107	–	0.61 ¹⁵¹	–	–																	
108	–	0.75 ¹⁵¹	–	–																	
109	–	2.9 ¹⁵²	–	–																	
110	–	9.8 ¹⁵³	–	AlkB (> 50) ¹⁵³ ALKBH2 (>50) ¹⁵³	 <table border="1" data-bbox="933 556 1339 640"> <thead> <tr> <th></th> <th>R¹</th> <th>R²</th> <th>R³</th> </tr> </thead> <tbody> <tr> <td>110</td> <td></td> <td>Cl</td> <td></td> </tr> <tr> <td>111</td> <td></td> <td></td> <td>CH₃</td> </tr> <tr> <td>112</td> <td></td> <td></td> <td></td> </tr> </tbody> </table>		R ¹	R ²	R ³	110		Cl		111			CH ₃	112			
	R ¹	R ²	R ³																		
110		Cl																			
111			CH ₃																		
112																					
111	–	32.3 ¹⁵³	–	–																	
112	–	13.1 ¹⁵³	–	–																	
113	–	0% ¹⁵⁴	–	AlkB (19.37) ¹⁵⁴	 <table border="1" data-bbox="933 787 1339 850"> <thead> <tr> <th></th> <th>R¹</th> <th>R²</th> <th>R³</th> </tr> </thead> <tbody> <tr> <td>113</td> <td></td> <td>Cl</td> <td>Ph</td> </tr> </tbody> </table>		R ¹	R ²	R ³	113		Cl	Ph								
	R ¹	R ²	R ³																		
113		Cl	Ph																		
114	4.9 ¹⁵⁵	–	–	–	 <p> 114 R = CH₃ 115 R = CH₂CH₃ </p>																
115	8.7 ¹⁵⁵	–	–	–																	
116	27.79 ¹⁵⁶	–	–	–	 <p>116 Clausine E</p>																
117	24.65 ¹⁵⁷	–	–	–	 <p>117</p>																
118	–	–	–	AlkB (80) ¹²⁴	 <p>118 Quercetin</p>																
119	–	–	Increase in m ⁶ A in RNA: at 10 μM (>50%) ¹⁵⁹ at 25 μM (>200%) ¹⁵⁹	–	 <p>119 MV1035</p>																
120	–	–	0.84 ¹⁶⁰	–	 <p>120</p>																
121	–	–	1.79 ¹⁶⁰	–	 <p>121</p>																

= 0.34 μM), **98** (IC_{50} = 0.49 μM) and **99** (IC_{50} = 0.85 μM), exhibit sub-micromolar potencies against FTO and are able to modulate m⁶A methylation levels in cellular RNA.¹³⁹ Several others are selective for FTO over ALKBH5. Compounds **99** and **102** in particular, exhibits more than 15-fold selectivity for FTO over ALKBH5. Notably, although metizoline **95** is 2.8-fold less potent than its analogue **98**, it has the advantage of reduced toxicity and improved pharmacokinetic profile.¹³⁹

Benzimidazole, pyrazole and indenone derivatives. In an effort to develop an anti-prostate cancer drug that target ALKBH3,^{63,150} Tanaka *et al.* randomly screened a library consisting of 17,000 commercially-available compounds, which led to the identification of benzimidazole compound **104** as a promising ALKBH3 inhibitor (Table 10).¹⁵¹ Subsequent structural optimisation of **104** led to a series of analogues **105-109** with remarkable sub-micromolar potency against ALKBH3, many of which are able to inhibit the proliferation of prostate cancer DU145 cell lines in cell culture.^{151,152} HUHS015 **105**, in particular, showed good oral-availability (bioavailability of 7.2% in rats after oral administration) and found to significantly suppress the growth of a human DU145 prostate cancer cells in a mouse xenograft model, with no observed side effects.¹⁵²

Recently, Anindya and Khan *et al.* tested a series of indenone derivatives for activity against ALKBH3 (selected examples are given in Table 10).¹⁵³ The indanone scaffold is of particular interest because it is present in a range of natural products, including euplectin, pauciflorol-F and neolignans. Most indanone derivatives investigated by the group exhibit poor ALKBH3 inhibition (IC_{50} 's > 50 μM), the most potent compounds are **110** (IC_{50} = 9.8 μM) and **112** (IC_{50} = 13.1 μM).¹⁵³ Further biochemical analyses found that **110** is about 5-fold more selective for ALKBH3 over AlkB and ALKBH2, and it is able to inhibit the growth and proliferation of human lung cancer A549 cell line.¹⁵³ Notably, **113** showed no detectable activity against ALKBH3, but exhibit moderate AlkB inhibition (IC_{50} = 19.37 μM ; Table 10),¹⁵⁴ suggesting that judicious placement of substituents on the indanone scaffold can drive selectivity for a particular AlkB subfamily member.

Other scaffolds that have been reported as FTO inhibitors include dihydroxyfuran sulphonamides **114-115**,¹⁵⁵ Clausine E **116**¹⁵⁶ and 2-phenyl benzimidazole **117**.¹⁵⁷ The selectivity and cellular activity of these compounds have not been determined. The flavonoid quercetin **118** was also reported to inhibit AlkB.¹²⁴

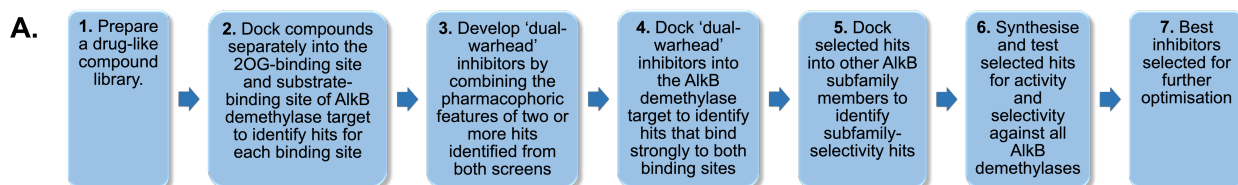
Recently, several cell-active ALKBH5 inhibitors have been reported. One notable example is **ALK-04** (chemical structure not reported). This compound was identified through a combined approach using *in silico* screening and SAR studies on a library of synthesised compounds.¹⁵⁸ The mode of binding of **ALK-04** is unknown at present. *In vitro* cytotoxicity studies found that **ALK-04** is non-toxic to cells and does not significantly affect the proliferation of B16 cells at concentrations up to 50 μM .¹⁵⁸ Moreover, mice treated with **ALK-04** showed significantly reduced tumour growth compared to control.¹⁵⁸ **ALK-04** also enhances the anticancer efficacy of GVAX/anti-PD-1 immunotherapy against melanoma, likely by modifying m⁶A levels and splicing of m⁶A-

regulated genes.¹⁵⁸ Considering the ALKBH5 gene mutation and expression status of melanoma patients correlate with their response to immunotherapy, small-molecule inhibitors of ALKBH5 may enhance the efficacy of anti-cancer immunotherapy.

Another notable example is the imidazobenzoxazin-5-thione compound MV1035 (**119**; Table 10).¹⁵⁹ This compound was originally designed as a sodium channel blocker but was subsequently identified as an ALKBH5 inhibitor *via* a proteome-wide structure-based *in silico* screening approach. Computational modelling studies suggest that **119** likely binds to a region deep within ALKBH5, in close proximity to the 2OG-binding site of ALKBH5 and partially overlap with the site occupied by the carboxylate group of 2OG.¹⁵⁹ *In vitro* dot plot assay showed that **119** is able to inhibit the activity of ALKBH5, leading to a significant increase in the levels of m⁶A in m⁶A-ssRNA in a dose-dependent manner.¹⁵⁹ In addition, cell-based assay showed that a concentration of 10 μM **119** is sufficient to reduce the proliferation and invasiveness of U87 glioblastoma cell line.¹⁵⁹ This is associated with a reduction of the expression of CD73 (an extrinsic protein involved in the generation of adenosine which is overexpressed in glioblastoma cells) without altering CD73 transcription.¹⁵⁹

Compounds **120** (IC_{50} = 0.84 μM ; Table 10) and **121** (IC_{50} = 1.79 μM ; Table 10) were also identified through a high-throughput virtual library screen, and were subsequently verified as highly potent ALKBH5 inhibitors using an m⁶A antibody-based enzyme-linked immunosorbent assay.¹⁶⁰ The precise mode of binding of these inhibitors are unknown, however molecular docking studies suggest that both **120** and **121** likely occupy the 2OG-binding site of ALKBH5.¹⁶⁰ In the case of **120**, strong hydrogen-bonding interactions were identified 1) between the C-5 carboxylate group of **120** and the side chain of Asn193, and 2) between the C-2 hydroxyl group of **120** and the side chain of Asp206.¹⁶⁰ 3) The C-2 hydroxyl group further participates in water-mediated hydrogen-bonding with Arg283. 4) Additional hydrophobic interaction was also identified between the phenyl group and the imidazole ring of His266.¹⁶⁰ The multiple interactions provide a rationale for the sub-micromolar potency of **120** against ALKBH5. Cell-based experiments found that **120** and **121** were able to significantly suppress the proliferation of three leukaemia cell lines (HL-60, CCRF-CEM, and K562), with IC_{50} values ranging from 1.38 μM to 16.5 μM ,¹⁶⁰ suggesting that these inhibitors may be promising leads for the development of novel anti-cancer treatment.

Screening strategy for selective AlkB demethylase inhibitors. The identification of numerous co-crystal structures has provided rich structural insights into the different modes of binding of the AlkB demethylase inhibitors. Detailed crystallographic analyses revealed a number of shared pharmacophores and highly-conserved interactions with the 2OG-binding site and substrate-binding site. These key interactions are summarised in Figure 6. In light of the recent discovery of dual-binding FTO inhibitor, LipotF **23**,¹⁰⁶ which exploits binding to both binding sites to achieve remarkable potency and subfamily-selectivity, we envisaged that a similar strategy could enable the selective



B.

Highly-conserved interactions between AlkB demethylases and reported inhibitors

Binding site	FTO	ALKBH1*	ALKBH2*	ALKBH3*	ALKBH5*	ALKBH7*	ALKBH8*
2OG-binding site#	Arg316 participates in: salt bridge interaction with -COOH in LipotF 23 , citrate 7 , 2,4-PDCA 15 , NOG 1 , IOX1 32 , IOX3 35 , 20	Arg338	Arg248	Arg269	Arg277	Arg197	Arg328
	Arg322 participates in: hydrogen bonding with C=O/-COOH/-OH in 2,4-PDCA 15 , NOG 1 , rhein 52 , fluorescein 65 , 67	Arg344	Arg254	Arg275	Arg283	Arg203	Arg334
	Asn205 participates in: hydrogen bonding with -COOH/-OH/C=O in citrate 7 , NOG 1 , 20 , entacapone 87	Asn220	Asn159	Asn179	Asn193	Led110	Asn227
	Ser318 participates in: hydrogen bonding with -COOH in LipotF 23 , 2,4-PDCA 15 , NOG 1 , IOX1 32 , IOX3 35 , 20	Asn340	Asn250	Asn271	Val279	Ser199	Ser330
	Tyr295 participates in: hydrogen bonding with -COOH in LipotF 23 , 2,4-PDCA 15 , NOG 1 , IOX3 35 , 20	Met276	Leu224	Leu254	Thr254	Tyr165	Leu280
Substrate-binding site	Arg96 participates in: hydrogen bonding with -COOH/-OH in 24PDCA 15 , NOG 1 , rhein 52 , fluorescein 65 , 67 cation-dipole interaction with -Cl in meclofenamic acid 59 , FB23 60	n.a.	Gln112	Arg131	Lys132	Glu75	Val176
	Ser229 participates in: hydrogen bonding with -COOH in rhein 52 , meclofenamic acid 59 , FB23 60 , fluorescein 65 , 67 water-mediated hydrogen bonding with CDPCB 75 and CHTB 85 Van der Waals contact with -Cl in CDPCB 75 Non-conventional hydrogen bond with -CH ₃ in CHTB 85	n.a.	Cys169	Asp189	Val202	Lys119	Pro236
	Glu234 (amide backbone) participates in: hydrogen bonding with pyridyl nitrogen/-OH/nitrogen or oxygen atom of heterocyclic ring in LipotF 23 , CHTB 85 water-mediated bond, FB23 60	Arg234	Glu175	Glu195	Glu153	Ser124	Thr241
	His231 participates in: π - π interactions with -C ₆ H ₅ in rhein 52 , CHTB 85 , LipotF 23	His231	His171	His191	His204	His121	His238
	His232 (carbonyl backbone) participates in: hydrogen bonding with -OH in CHTB 85	Val232	Arg172	Ser192	Val205	Val122	Ile239
	Tyr108 participates in: π - π interactions with -C ₆ H ₅ in LipotF 23	Tyr177	Phe124	Tyr143	Tyr139	Asp67	n.a.
	Tyr106 participates in: hydrogen bonding with -OH in entacapone 87	Tyr184	Tyr122	Pro140	Phe211	Trp66	Phe245
	Leu109 participates in: hydrophobic interactions with -C ₆ H ₅ in LipotF 23 , fluorescein 65 , 67 , CHTB 85	n.a.	Ser125	n.a.	Tyr141	n.a.	n.a.
	Leu91 (carbonyl backbone) participates in: hydrogen bonding with -NH ₂ in fluorescein 65 , 67	n.a.	Ser107	Gln128	n.a.	n.a.	n.a.
	Leu90, Ile85, Pro93 participates in: hydrophobic interactions with -C ₆ H ₅ in meclofenamic acid 59 , CDPCB 75 , fluorescein 65 , 67 , CHTB 85	n.a.	His106	Tyr127	Arg130	His65	n.a.
	Ile85 participates in: Van der Waals contact with gem dimethyl group in CHTB 85	n.a.	Val101	Arg122	Pro128	Asp67	n.a.
	Lys216 (amide backbone) participates in: hydrogen bonding with -OH in CDPCB 75	n.a.	Cys169	n.a.	n.a.	Lys119	n.a.
	Met226 (carbonyl backbone) participates in: hydrogen bonding with -OH in CDPCB 75 , Van der Waals contact with -Cl in CDPCB 75	Phe27	n.a.	Arg258	Gln233	n.a.	n.a.
	Val228 participates in: hydrophobic interactions with -C ₆ H ₅ in LipotF 23	Leu228	Ile168	Val188	Ile201	Ile118	Ile235
	Val94 (amide backbone) participates in: hydrogen bonding with -OH in CHTB 85	n.a.	Arg110	Arg131	Tyr195	n.a.	Arg174

Figure 6. The *in silico* 'dual warhead' screening strategy for the discovery of selective AlkB demethylase inhibitors. (A) This strategy exploits binding to both the 2OG-binding site and substrate-binding site to confer potency and selectivity, respectively. **(B)** Crystallographic analysis of reported AlkB demethylase inhibitors revealed a number of highly-conserved interactions with the 2OG-binding site and substrate-binding site. #Interaction of inhibitors with Fe(II) in the 2OG-binding site have been omitted. *The equivalent residues for each AlkB subfamily members are shown; n.a. denotes no equivalent residues.

inhibition of other AlkB subfamilies. Hence, an *in silico* 'dual warhead' inhibitor screening strategy could begin with 1) the preparation of a drug-like compound library, which is then docked into the 2OG-binding site of the AlkB demethylase target. The first round of docking seeks to identify hits that are able to bind strongly to the 2OG-binding site, focusing on the highly-conserved interactions outlined in Figure 6B. 2) The second round of inhibitor screening focuses on identifying compounds with a strong binding affinity to the substrate-binding site and their ability to participate in key interactions highlighted in Figure 6B. 3) 'Dual warheads' inhibitors are then developed by combining or merging the pharmacophoric features of two or more hits identified from both screening campaigns. 4) The hybrid inhibitors are then docked into the target AlkB demethylase to assess their ability to bind to both binding sites. 5) Selected hits are further docked into other AlkB subfamily members to evaluate their subfamily-selectivity. 6) Compounds that bind strongly to both binding sites and exhibit favourable selectivity profile are then synthesised and tested for activity against all AlkB demethylases. 7) The best inhibitors are selected as leads for further optimisation through medicinal chemistry efforts (Figure 6A).

5. PERSPECTIVES

Over the past decades, we have witnessed tremendous advances in the development of AlkB demethylase inhibitors, principally aimed at improving their selectivity and cellular activity. These medicinal chemistry efforts have been massively facilitated by a number of significant breakthroughs in this field. One major step forward is the development of several high-throughput methyl-specific sequencing methods,¹⁶¹⁻¹⁶⁹ such as bisulphite sequencing and methylated RNA immunoprecipitation sequencing (MeRIP) techniques, which has enabled genome-wide and transcriptome-wide mapping of the methylome landscape and, subsequently, the identification of physiological substrates for the AlkB subfamily members. This development has also led to the development of a range of biochemical¹⁷⁰⁻¹⁷⁴ and cell-based^{175,176} demethylase assay methods, which greatly facilitated the functional and inhibition studies of these fascinating enzymes. Extensive crystallography work further provided unprecedented insights into the catalytic mechanisms of the AlkB demethylases, and molecular details of their substrate recognition and specificity.⁹⁰⁻⁹⁷ Indeed, the availability of these high-resolution crystal structures represents a major step change in our approach to AlkB demethylase inhibition research, enabling better inhibitor design through structure-based and computationally-guided methods.

Despite these advances, inhibition work on AlkB demethylases is still at a relatively early stage from a medicinal chemistry perspective, at least compared to other Fe(II)/2OG-dependent oxygenases, particularly the PHDs and JmjC KDMs. Nevertheless, the successful discovery of reasonably potent and selective inhibitors against several AlkB demethylases, in particular AlkB, FTO, ALKBH3 and ALKBH5 suggests that the AlkB family as a whole is amenable to small molecule inhibition. Moreover, currently available results indicate that chemical inhibition of these

enzymes is not highly toxic, hence the AlkB demethylases could be promising targets for novel epigenetic therapy.

More than a hundred small-molecule inhibitors of AlkB demethylases have been reported to date, many of which, particularly the early inhibitors, are 2OG-competitive inhibitors that chelate to iron in the 2OG-binding site. Whilst the majority of inhibitors from this class exhibit a broad spectrum of activities, compounds that are highly selective for AlkB (*e.g.* **19**), FTO (*e.g.* **43**) and ALKBH3 (*e.g.* **44**) have been reported, which is remarkable given the high levels of structural similarities of the 2OG binding sites amongst the AlkB subfamilies. The result suggests that selective inhibition of the AlkB subfamilies is achievable by exploiting the 2OG-binding site alone.

Another major class of inhibitors is the 'substrate competitors'. Inhibitors from this class exploit differences in the nucleotide-binding sites for selective targeting of AlkB subfamily members. A number of compounds from this class (*e.g.* **59** and **65**) bind to the nucleotide recognition lid, which is a unique structural feature of the AlkB demethylases not found in other Fe(II)/2OG-dependent oxygenases. Recently, 'dual warhead' compounds have been developed, which occupy both the 2OG-binding site and nucleotide-binding site simultaneously, thus able to competitively inhibit the binding of co-substrate and substrate. This is exemplified by the subfamily-selective and cell-active FTO inhibitor LipotF **23** and entacapone **87**.

Interestingly, several natural products, such as rhein **52** and radicicol **86**, have also been identified through high-throughput screening as relatively potent inhibitors of FTO. Although these compounds also target a range of other human proteins, hence unlikely to be useful as functional probes, their structural diversity provides fresh inspiration for novel inhibitor scaffolds. Notably, several FDA-approved drugs that are currently in clinical use, such as meclizemine **59** and entacapone **87**, have also been shown to inhibit FTO in cells, leading to a significant increase in cellular m⁶A levels. This result suggests that the pharmacological actions of these drugs may be mediated, at least in part, by FTO inhibition. The clinical implication of this finding may warrant further investigation.

Despite significant progress in this field, a number of important challenges remain. To date, the structures of ALKBH4 and ALKBH6 have not been defined. The molecular basis for the recognition of several substrates by AlkB demethylases also remains unknown. For instance, it is not clear how FTO specifically recognise m¹A base modification in tRNA. The exact mode of binding of ALKBH5 with dimethylated adenosine m⁶2A, and the interaction of ALKBH1 with actin protein have yet to be determined. Furthermore, majority of the inhibition work to date have focused on FTO and ALKBH3. Whilst small-molecule inhibitors have been reported for AlkB, ALKBH2 and ALKBH5, none exhibit subfamily-selectivity which is essential for functional assignments and target validation. At present, inhibition of other AlkB subfamily members has not been achieved. It is desirable to develop new classes of inhibitors with novel mode of binding, particularly those that target previously unexplored structural domains. In this regards, subfamily-specific structural elements, such as the methyltransferase

domain of ALKBH8 and the C-terminal domain of FTO may provide opportunities for the design of subfamily-selective inhibitors. In light that several natural products are reasonably potent inhibitors of FTO, we envisaged that natural product-inspired inhibitors will gain traction in the years to come. Given the wealth of crystallographic information currently available, a challenge will be to apply them to the discovery of selective inhibitors for each and every member of this medically-important class of enzymes.

AUTHOR INFORMATION

Corresponding Author

* **Esther C. Y. Woon** – School of Pharmacy, University College London, 29-39 Brunswick Square, London WC1N 1AX, United Kingdom; orcid.org/0000-0001-7501-2872; Email: e.woon@ucl.ac.uk

Authors

Gemma S. Perry – School of Pharmacy, University College London, 29-39 Brunswick Square, London WC1N 1AX, United Kingdom; orcid.org/0000-0002-8002-375X

Mohua Das – Lab of Precision Oncology and Cancer Evolution, Genome Institute of Singapore, 60 Biopolis Street, Singapore 138672, Singapore; orcid.org/0000-0002-8891-6333

Author Contributions

All authors contributed equally to this work.

Notes

The authors declare no competing financial interest.

Biographies

Gemma S. Perry is a PhD student at the University College London School of Pharmacy, where she is working in Dr Esther Woon's group investigating novel small molecule inhibitors for AlkB demethylases. She received her M.Sci. (Hons) in Natural Sciences from Durham University in 2019, where she worked on a project involving CO₂-dependent NF- κ B signalling, before spending two years in the pharmaceutical industry working on small molecule drug discovery for serine proteases.

Mohua Das is a postdoctoral fellow at the Genome Institute of Singapore. She received her Ph.D. degree from the National University of Singapore, where she worked on small-molecule probes for selective inhibition of AlkB demethylases. In her current role, she is focused on developing Wnt modulators to remodel the immune landscape in tumour microenvironment. She is also interested in studying the role of epitranscriptome in chemotherapy-induced drug resistance.

Esther C. Y. Woon is an Associate Professor of Epigenetic Drug Discovery at the University College London School of Pharmacy. Her research focuses on understanding the structure, mechanism, and function of novel epigenetic proteins, particularly the DNA/RNA demethylases, with a view to identifying novel disease targets and biomarkers. To enable this research, her lab has developed a range of drug discovery strategies and bioassays using smart fluorescent biosensors and nanomachines. Her research contributed to the first discovery of

inhibitors against several AlkB demethylases and JmjC histone demethylases, many of which are subfamily-selective and cell-active.

ACKNOWLEDGMENTS

We thank the University College London (Grant Award 156780), Singapore National Medical Research Council (NMRC/BNIG/2008/2013) and the Singapore Ministry of Education (AcRF Tier 1 Grant R148-000-231-114; AcRF Tier 1 Grants R148-000-238 114) for funding our work on AlkB demethylase inhibition. G. S. P. acknowledges a University College London postgraduate studentship. We apologise for incomplete citations due to space constraints. Patent applications were cited only where compound structures and information are not available in peer-reviewed literatures.

ABBREVIATIONS USED

1,*N*²- ϵ G, 1,*N*²-ethenoguanosine; 2,4-PDCA, 2,4-pyridine dicarboxylic acid; 2HG, 2-hydroxyglutarate; 2MG, 2-mercaptoglutamate; 2OG, 2-oxoglutarate; Ala, alanine residue; AML, acute myeloid leukaemia; Arg, arginine residue; Asn, asparagine residue; Asp, aspartic acid residue; CC, coiled-coil; cm⁵U, 5-carboxymethyluridine; COMT, catechol-*O*-methyltransferase; COX, cyclooxygenase; CTD, C-terminal domain; CYP, cytochrome P450; Cys, cysteine residue; DCC, multiprotein dynamic combinatorial chemistry; DCMS, dynamic combinatorial mass spectrometry; DFHBI-1T, 3,5-difluoro-4-hydroxybenzylidene 1-trifluoroethyl-imidazole; DMOG, dimethylxalylglycine; DSBH, double-stranded β -helix; dsDNA, double-stranded DNA; DSF, differential scanning fluorometric; DZ, diazine ring (DZ); EA, 1,*N*⁶-ethanoadenosine; *E. coli*, *Escherichia coli*; e¹A, *N*¹-ethyladenosine; e²G, *N*²-ethylguanosine; e³C, *N*³-ethylcytidine; FF, *N*²-furan-2-ylmethylguanosine; FH, fumarate hydratase; FIH, factor inhibiting HIF FOXO1, forkhead box protein O1; FTO, fat mass and obesity-associated protein; GB/SA, generalised born surface area; HDAC, histone deacetylase; HF, *N*²-tetrahydrofuran-2-yl-methylguanosine; HIF, hypoxia inducible factor; His, histidine residue; IDH, isocitrate dehydrogenase; Ile, isoleucine residue; JmjC, Jumonji C-terminal domain; KDM, histone lysine demethylase; Leu, leucine residue; Lys, lysine residue; m¹A, *N*¹-methyladenosine; m¹G, *N*¹-methylguanosine; m²G, *N*²-methylguanosine; m³C, *N*³-methylcytidine; m³T, *N*³-methylthymidine; m³U, *N*³-methyluridine; m⁴C, *N*⁴-methylcytidine; m⁵C, 5-methylcytidine; m⁶₂A, *N*⁶,*N*⁶-dimethyladenosine; m⁶A, *N*⁶-methyladenosine; m⁶Am, *N*⁶,2'-*O*-dimethyladenosine; MA, meclofenamic acid; mchm⁵U, (*S*)-5-methoxycarbonylmethyluridine; mcm⁵U, 5-methoxycarbonylmethyluridine; MeRIP, methylated RNA immunoprecipitation sequencing; Met, methionine residue; MM, molecular mechanics; MMS, methyl methane sulphonate; mRNA, messenger RNA; MT, methyltransferase domain; MTS, N-terminal mitochondrial targeting sequence; MUG, mismatch specific uracil DNA glycosylase; NASH, non-alcoholic steatohepatitis; NOG, *N*-oxalylglycine; NRL, nucleotide recognition lid; NTE, N-terminal extension; PCA-1, prostate cancer antigen-1; PHD, HIF prolyl hydroxylase; Phe, phenylalanine residue; PHF, PHD finger protein; Pro, proline residue; RRM, RNA recognition motif; rRNA, ribosomal RNA; SDH, succinate dehydrogenase; Ser, serine residue; ssDNA, single-stranded DNA; ssRNA, single-stranded RNA; TCA, tricarboxylic acid; TET1, ten-eleven translocation 1; Thr, threonine residue; tRNA, transfer RNA; Trp, tryptophan residue; Tyr, tyrosine residue; Val, valine residue; ϵ A, 1,*N*⁶-ethenoadenosine; ϵ C, 3,*N*⁴-ethenocytidine.

REFERENCES

- (1) Greenberg, M. V. C.; Bourc'his, D. The diverse roles of DNA methylation in mammalian development and disease. *Nat. Rev. Mol. Cell Biol.* **2019**, *20*, 590-607.
- (2) Grosjean, H. *Fine-tuning of RNA functions by modification and editing*, Vol. 12; Springer-Verlag: Berlin, Heidelberg, 2005.
- (3) Grosjean, H.; Benne, R. *Modification and Editing of rRNA*; ASM Press: Washington, D. C., USA, 1998.
- (4) Boccaletto, P.; Machnicka, M. A.; Purta, E.; Piatkowski, P.; Baginski, B.; Wirecki, T. K.; de Crécy-Lagard, V.; Ross, R.; Limbach, P. A.; Kotter, A.; Helm, M.; Bujnicki, J. M. MODOMICS: a database of RNA modification pathways. *Nucleic Acids Research* **2018**, *46*, D303-D307.
- (5) Grosjean, H. *DNA and RNA Modification Enzymes: Structure, Mechanism, Function and Evolution*; CRC Press: Boca Raton, USA, 2009.
- (6) Aravind, L.; Koonin, E. V. The DNA-repair protein AlkB, EGL-9, and leprecan define new families of 2-oxoglutarate- and iron-dependent dependent oxygenases. *Genome Biol.* **2001**, *2*, RESEARCH0007.1-RESEARCH0007.8.
- (7) Schofield, C. J.; Hausinger, R. P. *2-Oxoglutarate-Dependent Oxygenases*; Royal Society of Chemistry: Cambridge, UK, 2015.
- (8) Trewick, S. C.; Henshaw, T. F.; Hausinger, R. P.; Lindahl, T.; Sedgwick, B. Oxidative demethylation by *Escherichia coli* AlkB directly reverts DNA base damage. *Nature* **2002**, *419*, 174-178.
- (9) Falnes, P.; Johansen, R. F.; Seeberg, E. AlkB-mediated oxidative demethylation reverses DNA damage in *Escherichia coli*. *Nature* **2002**, *419*, 178-182.
- (10) Delaney, J. C.; Essigmann, J. M. Mutagenesis, genotoxicity, and repair of 1-methyladenine, 3-alkylcytosines, 1-methylguanine, and 3-methylthymine in AlkB *Escherichia coli*. *Proc. Natl. Acad. Sci. U.S.A.* **2004**, *101*, 14051-14056.
- (11) Delaney, J. C.; Smeester, L.; Wong, C.; Frick, L. E.; Taghizadeh, K.; Wishnok, J. S.; Drennan, C. L.; Samson, L. D.; Essigmann, J. M. AlkB reverses etheno DNA lesions caused by lipid oxidation in vitro and in vivo. *Nat. Struct. Mol. Biol.* **2005**, *12*, 855-860.
- (12) Li, D.; Delaney, J. C.; Page, M.; Yang, X.; Chen, A. S.; Wong, C.; Drennan, C. L.; Essigmann, J. M. Exocyclic carbons adjacent to the N6 of adenine are targets for oxidation by the *Escherichia coli* adaptive response protein AlkB. *J. Am. Chem.* **2012**, *134*, 8896-8901.
- (13) Li, D.; Fedeles, B. I.; Shrivastav, N.; Delaney, J. C.; Yang, X.; Wong, C.; Drennan, C. L.; Essigmann, J. M. Removal of N-alkyl modifications from N2-alkylguanine and N4-alkylcytosine in DNA by the adaptive response protein AlkB. *Chem. Res. Toxicol.* **2013**, *26*, 1182-1187.
- (14) Frick, L. E.; Delaney, J. C.; Wong, C.; Drennan, C. L.; Essigmann, J. M. Alleviation of 1,N6-ethanoadenine genotoxicity by the *Escherichia coli* adaptive response protein AlkB. *PNAS* **2007**, *104*, 755-760.
- (15) Chang, S. C.; Fedeles, B. I.; Wu, J.; Delaney, J. C.; Li, D.; Zhao, L.; Christov, P. P.; Yau, E.; Singh, V.; Jost, M.; Drennan, C. L.; Marnett, L. J.; Rizzo, C. J.; Levine, S. S.; Guengerich, F. P.; Essigmann, J. M. Next-generation sequencing reveals the biological significance of the N(2),3-ethenoguanine lesion in vivo. *Nucleic Acids Research* **2015**, *43*, 5489-5500.
- (16) Westbye, M. P.; Feyzi, E.; Aas, P. A.; Vågbo, C. B.; Talstad, V. A.; Kavli, B.; Hagen, L.; Sundheim, O.; Akbari, M.; Liabakk, N. B.; Slupphaug, G.; Otterlei, M.; Krokan, H. E. Human AlkB homologue 1 is a mitochondrial protein that demethylates 3-methylcytosine in DNA and RNA. *J. Biol. Chem.* **2008**, *283*, 25046-25056.
- (17) Müller, T. A.; Meek, K.; Hausinger, R. P. Human AlkB homologue 1 (ABH1) exhibits DNA lyase activity at abasic sites. *DNA Repair (Amst)* **2010**, *9*, 58-65.
- (18) Falnes, P. Repair of 3-methylthymine and 1-methylguanine lesions by bacterial and human AlkB proteins. *Nucleic Acids Research* **2004**, *32*, 6260-6267.
- (19) Liu, F.; Clark, W.; Luo, G.; Wang, X.; Fu, Y.; Wei, J.; Wang, X.; Hao, Z.; Dai, Q.; Zheng, G.; Ma, H.; Han, D.; Evans, M.; Klungland, A.; Pan, T.; He, C. ALKBH1-mediated tRNA demethylation regulates translation. *Cell* **2016**, *167*, 816-828.
- (20) Kawarada, L.; Suzuki, T.; Ohira, T.; Hirata, S.; Miyauchi, K.; Suzuki, T. ALKBH1 is an RNA dioxygenase responsible for cytoplasmic and mitochondrial tRNA modifications. *Nucleic Acids Research* **2017**, *45*, 7401-7415.
- (21) Tian, L.-F.; Liu, Y.-P.; Chen, L.; Tang, Q.; Wu, W.; Sun, W.; Chen, Z.; Yan, X.-X. Structural basis of nucleic acid recognition and 6mA demethylation by human ALKBH1. *Cell Res.* **2020**, *30*, 272-275.
- (22) Zhang, M.; Yang, S.; Nelakanti, R.; Zhao, W.; Liu, G.; Li, Z.; Liu, X.; Wu, T.; Xiao, A.; Li, H. Mammalian ALKBH1 serves as an N6-mA demethylase of unpairing DNA. *Cell Res.* **2020**, *30*, 197-210.
- (23) Duncan, T.; Trewick, S. C.; Koivisto, P.; Bates, P. A.; Lindahl, T.; Sedgwick, B. Reversal of DNA alkylation damage by two human dependent oxygenases. *Proc. Natl. Acad. Sci. U.S.A.* **2002**, *99*, 16660-16665.
- (24) Aas, P. A.; Otterlei, M.; Falnes, P. O.; Vågbo, C. B.; Skorpen, F.; Akbari, M.; Sundheim, O.; Bjørås, M.; Slupphaug, G.; Seeberg, E.; Krokan, H. E. Human and bacterial oxidative demethylases repair alkylation damage in both RNA and DNA. *Nature* **2003**, *421*, 859-863.
- (25) Monsen, V. T.; Sundheim, O.; Aas, P. A.; Westbye, M. P.; Sousa, M. M.; Slupphaug, G.; Krokan, H. E. Divergent β -hairpins determine double-strand versus single-strand substrate recognition of human AlkB-homologues 2 and 3. *Nucleic Acids Research* **2010**, *38*, 6447-6455.
- (26) Koivisto, P.; Robins, P.; Lindahl, T.; Sedgwick, B. Demethylation of 3-methylthymine in DNA by bacterial and human DNA dioxygenases. *J. Biol. Chem.* **2004**, *279*, 40470-40474.
- (27) Zdzalik, D.; Domańska, A.; Prorok, P.; Kosicki, K.; van den Born, E.; Falnes, P. Ø.; Rizzo, C. J.; Guengerich, F. P.; Tudek, B. Differential repair of etheno-DNA adducts by bacterial and human AlkB proteins. *DNA Repair* **2015**, *30*, 1-10.
- (28) Chen, Z.; Qi, M.; Shen, B.; Luo, G.; Wu, Y.; Li, J.; Lu, Z.; Zheng, Z.; Dai, Q.; Wang, H. Transfer RNA demethylase ALKBH3 promotes cancer progression via induction of tRNA-derived small RNAs. *Nucleic Acids Research* **2019**, *47*, 2533-2545.
- (29) Bian, K.; Lenz, S. A. P.; Tang, Q.; Chen, F.; Qi, R.; Jost, M.; Drennan, C. L.; Essigmann, J. M.; Wetmore, S. D.; Li, D. DNA repair enzymes ALKBH2, ALKBH3, and AlkB oxidize 5-methylcytosine to 5-hydroxymethylcytosine, 5-formylcytosine and 5-carboxylcytosine in vitro. *Nucleic Acids Research* **2019**, *47*, 5522-5529.
- (30) Li, M.-M.; Nilsen, A.; Shi, Y.; Fusser, M.; Ding, Y.-H.; Fu, Y.; Liu, B.; Niu, Y.; Wu, Y.-S.; Huang, C.-M.; Olofsson, M.; Jin, K.-X.; Lv, Y.; Xu, X.-Z.; He, C.; Dong, M.-Q.; Rendtleg Danielsen, J. M.; Klungland, A.; Yang, Y.-G. ALKBH4-dependent demethylation of actin regulates actomyosin dynamics. *Nature Commun.* **2013**, *4*, 1832-1845.
- (31) Kweon, S.-M.; Chen, Y.; Moon, E.; Kvederaviciūtė, K.; Klimasauskas, S.; Feldman, D. E. An adversarial DNA N6-methyladenine-sensor network preserves polycomb silencing. *Mol. Cell* **2019**, *74*, 1138-1147.
- (32) Jia, G.; Fu, Y.; Zhao, X.; Dai, Q.; Zheng, G.; Yang, Y.; Yi, C.; Lindahl, T.; Pan, T.; Yang, Y.-G.; He, C. N6-methyladenosine in nuclear RNA is a major substrate of the obesity-associated FTO. *Nature Chem. Biol.* **2011**, *7*, 885-887.
- (33) Wei, J.; Liu, F.; Lu, Z.; Fei, Q.; Ai, Y.; He, P. C.; Shi, H.; Cui, X.; Su, R.; Klungland, A.; Jia, G.; Chen, J.; He, C. Differential m6A, m6Am, and m1A demethylation mediated by FTO in the cell nucleus and cytoplasm. *Mol. Cell* **2018**, *71*, 973-985.
- (34) Mauer, J.; Jaffrey, S. R. FTO, m6Am, and the hypothesis of reversible epitranscriptomic mRNA modifications. *FEBS Lett.* **2018**, *592*, 2012-2022.
- (35) Gerken, T.; Girard, C. A.; Tung, Y. C.; Webby, C. J.; Saudek, V.; Hewitson, K. S.; Yeo, G. S.; McDonough, M. A.; Cunliffe, S.; McNeill, L. A.; Galvanovskis, J.; Rorsman, P.; Robins, P.; Prieur, X.

- Coll, A. P.; Ma, M.; Jovanovic, Z.; Farooqi, I. S.; Sedgwick, B.; Barroso, I.; Lindahl, T.; Ponting, C. P.; Ashcroft, F. M.; O'Rahilly, S.; Schofield, C. J. The obesity-associated FTO gene encodes a 2-oxoglutarate-dependent nucleic acid demethylase. *Science* **2007**, *318*, 1469-1472.
- (36) Jia, G.; Yang, C.-G.; Yang, S.; Jian, X.; Yi, C.; Zhou, Z.; He, C. Oxidative demethylation of 3-methylthymine and 3-methyluracil in single-stranded DNA and RNA by mouse and human FTO. *FEBS Lett.* **2008**, *582*, 3313-3319.
- (37) Zheng, G.; Dahl, J. A.; Niu, Y.; Fedorcsak, P.; Huang, C. M.; Li, C. J.; Vågbo, C. B.; Shi, Y.; Wang, W. L.; Song, S. H.; Lu, Z.; Bosmans, R. P.; Dai, Q.; Hao, Y. J.; Yang, X.; Zhao, W. M.; Tong, W. M.; Wang, X. J.; Bogdan, F.; Furu, K.; Fu, Y.; Jia, G.; Zhao, X.; Liu, J.; Krokan, H. E.; Klungland, A.; Yang, Y. G.; He, C. ALKBH5 is a mammalian RNA demethylase that impacts RNA metabolism and mouse fertility. *Mol. Cell* **2013**, *49*, 18-29.
- (38) Feng, C.; Liu, Y.; Wang, G.; Deng, Z.; Zhang, Q.; Wu, W.; Tong, Y.; Cheng, C.; Chen, Z. Crystal structures of the human RNA demethylase Alkbh5 reveal basis for substrate recognition. *J. Biol. Chem.* **2014**, *289*, 11571-11583.
- (39) Xu, C.; Liu, K.; Tempel, W.; Demetriades, M.; Aik, W.; Schofield, C. J.; Min, J. Structures of human ALKBH5 demethylase reveal a unique binding mode for specific single-stranded N6-methyladenosine RNA demethylation. *J. Biol. Chem.* **2014**, *289*, 17299-17311.
- (40) Zou, S.; Toh, J. D. W.; Wong, K. H. Q.; Gao, Y.-G.; Hong, W.; Woon, E. C. Y. N6-Methyladenosine: a conformational marker that regulates the substrate specificity of human demethylases FTO and ALKBH5. *Sci. Rep.* **2016**, *6*, 25677-25689.
- (41) Frayling, T. M.; Timpson, N. J.; Weedon, M. N.; Zeggini, E.; Freathy, R. M.; Lindgren, C. M.; Perry, J. R.; Elliott, K. S.; Lango, H.; Rayner, N. W.; Shields, B.; Harries, L. W.; Barrett, J. C.; Ellard, S.; Groves, C. J.; Knight, B.; Patch, A. M.; Ness, A. R.; Ebrahim, S.; Lawlor, D. A.; Ring, S. M.; Ben-Shlomo, Y.; Jarvelin, M. R.; Sovio, U.; Bennett, A. J.; Melzer, D.; Ferrucci, L.; Loos, R. J.; Barroso, I.; Wareham, N. J.; Karpe, F.; Owen, K. R.; Cardon, L. R.; Walker, M.; Hitman, G. A.; Palmer, C. N.; Doney, A. S.; Morris, A. D.; Smith, G. D.; Hattersley, A. T.; McCarthy, M. I. A common variant in the FTO gene is associated with body mass index and predisposes to childhood and adult obesity. *Science* **2007**, *316*, 889-894.
- (42) Smemo, S.; Tena, J. J.; Kim, K. H.; Gamazon, E. R.; Sakabe, N. J.; Gómez-Marín, C.; Aneas, I.; Credidio, F. L.; Sobreira, D. R.; Wasserman, N. F.; Lee, J. H.; Puvion-Dran, V.; Tam, D.; Shen, M.; Son, J. E.; Vakili, N. A.; Sung, H. K.; Naranjo, S.; Acemel, R. D.; Manzanares, M.; Nagy, A.; Cox, N. J.; Hui, C. C.; Gomez-Skarmeta, J. L.; Nóbrega, M. A. Obesity-associated variants within FTO form long-range functional connections with IRX3. *Nature* **2014**, *507*, 371-375.
- (43) Claussnitzer, M.; Dankel, S. N.; Kim, K. H.; Quon, G.; Meuleman, W.; Haugen, C.; Glunk, V.; Sousa, I. S.; Beaudry, J. L.; Puvion-Dran, V.; Abdennur, N. A.; Liu, J.; Svensson, P. A.; Hsu, Y. H.; Drucker, D. J.; Mellgren, G.; Hui, C. C.; Hauner, H.; Kellis, M. FTO Obesity Variant Circuitry and Adipocyte Browning in Humans. *N. Engl. J. Med.* **2015**, *373*, 895-907.
- (44) Yang, P.; Wang, Q.; Liu, A.; Zhu, J.; Feng, J. ALKBH5 holds prognostic values and inhibits the metastasis of colon cancer. *Pathol. Oncol. Res.* **2020**, *26*, 1615-1623.
- (45) Ensfielder, T. T.; Kurz, M. Q.; Iwan, K.; Geiger, S.; Matheisl, S.; Müller, M.; Beckmann, R.; Carell, T. ALKBH5-induced demethylation of mono- and dimethylated adenosine. *Chem. Commun.* **2018**, *54*, 8591-8593.
- (46) Fu, Y.; Dai, Q.; Zhang, W.; Ren, J.; Pan, T.; He, C. The AlkB domain of mammalian ABH8 catalyses hydroxylation of 5-methoxycarbonylmethyluridine at the wobble position of tRNA. *Angew. Chem. Int. Ed.* **2010**, *49*, 8885-8888.
- (47) Huang, T. T.; Ngoc, L. N.; Kang, H. Functional characterization of a putative RNA demethylase ALKBH6 in Arabidopsis growth and abiotic stress responses. *Int. J. Mol. Sci.* **2020**, *21*, 6707-6721.
- (48) Wang, G.; He, Q.; Feng, C.; Liu, Y.; Deng, Z.; Qi, X.; Wu, W.; Mei, P.; Chen, Z. The atomic resolution structure of human AlkB homologue 7 (ALKBH7), a key protein for programmed necrosis and fat metabolism. *J. Biol. Chem.* **2014**, *289*, 27924-27936.
- (49) Roundtree, I. A.; Evans, M. E.; Pan, T.; He, C. Dynamic RNA modifications in gene expression regulation. *Cell* **2017**, *169*, 1187-1200.
- (50) He, P. C.; He, C. m6A RNA methylation: from mechanisms to therapeutic potential. *EMBO J.* **2021**, *40*, e105977.
- (51) Jiang, X.; Liu, B.; Nie, Z.; Duan, L.; Xiong, Q.; Jin, Z. The role of m6A modification in the biological functions and diseases. *Sig. Transduct. Target. Ther.* **2021**, *6*, 74-90.
- (52) Yang, C.; Hu, Y.; Zhou, B.; Bao, Y.; Li, Z.; Gong, C. The role of m6A modification in physiology and disease. *Cell Death Dis.* **2020**, *11*, 960-976.
- (53) Freathy, R. M.; Timpson, N. J.; Lawlor, D. A.; Pouta, A.; Ben-Shlomo, Y.; Ruukonen, A.; Ebrahim, S.; Shields, B.; Zeggini, E.; Weedon, M. N.; Lindgren, C. M.; Lango, H.; Melzer, D.; Ferrucci, L.; Paolisso, G.; Neville, M. J.; Karpe, F.; Palmer, C. N.; Morris, A. D.; Elliott, P.; Jarvelin, M. R.; Smith, G. D.; McCarthy, M. I.; Hattersley, A. T.; Frayling, T. M. Common variation in the FTO gene alters diabetes-related metabolic traits to the extent expected given its effect on BMI. *Diabetes* **2008**, *57*, 1419-1426.
- (54) Scuteri, A.; Sanna, S.; Chen, W. M.; Uda, M.; Albai, G.; Strait, J.; Najjar, S.; Nagaraja, R.; Orrú, M.; Usala, G.; Dei, M.; Lai, S.; Maschio, A.; Busonero, F.; Mulas, A.; Ehret, G. B.; Fink, A. A.; Weder, A. B.; Cooper, R. S.; Galan, P.; Chakravarti, A.; Schlessinger, D.; Cao, A.; Lakatta, E.; Abecasis, G. R. Genome-wide association scan shows genetic variants in the FTO gene are associated with obesity-related traits. *PLoS Genet.* **2007**, *3*, 1200-1210.
- (55) Keller, L.; Xu, W.; Wang, H. X.; Winblad, B.; Fratiglioni, L.; Graff, C. The obesity related gene, FTO, interacts with APOE, and is associated with Alzheimer's disease risk: a prospective cohort study. *J. Alzheimers Dis.* **2011**, *23*, 461-469.
- (56) Reitz, C.; Tosto, G.; Mayeux, R.; Luchsinger, J. A. Genetic variants in the fat and obesity associated (FTO) gene and risk of Alzheimer's disease. *PLoS One* **2012**, *7*, e50354.
- (57) Lim, A.; Zhou, J.; Sinha, R. A.; Singh, B. K.; Ghosh, S.; Lim, K.-H.; Chow, P. K. H.; Woon, E. C. Y.; Yen, P. M. Hepatic FTO expression is increased in NASH and its silencing attenuates palmitic acid-induced lipotoxicity. *Biochem. Biophys. Res. Commun.* **2016**, *479*, 476-481.
- (58) Li, Y.; Zheng, D.; Wang, F.; Xu, Y.; Yu, H.; Zhang, H. Expression of demethylase genes, FTO and ALKBH1, is associated with prognosis of gastric cancer. *Dig. Dis. Sci.* **2019**, *64*, 1503-1513.
- (59) Xie, Q.; Wu, T. P.; Gimple, R. C.; Li, Z.; Prager, B. C.; Wu, Q.; Yu, Y.; Wang, P.; Wang, Y.; Gorkin, D. U.; Zhang, C.; Dowiak, A. V.; Lin, K.; Zeng, C.; Sui, Y.; Kim, L. J. Y.; Miller, T. E.; Jiang, L.; Lee, C. H.; Huang, Z.; Fang, X.; Zhai, K.; Mack, S. C.; Sander, M.; Bao, S.; Kerstetter-Fogle, A. E.; Sloan, A. E.; Xiao, A. Z.; Rich, J. N. N(6)-methyladenine DNA modification in glioblastoma. *Cell* **2018**, *175*, 1228-1243.
- (60) Fujii, T.; Shimada, K.; Anai, S.; Fujimoto, K.; Konishi, N. ALKBH2, a novel AlkB homologue, contributes to human bladder cancer progression by regulating MUC1 expression. *Cancer Sci.* **2013**, *104*, 321-327.
- (61) Yamato, I.; Sho, M.; Shimada, K.; Hotta, K.; Ueda, Y.; Yasuda, S.; Shigi, N.; Konishi, N.; Tsujikawa, K.; Nakajima, Y. PCA-1/ALKBH3 contributes to pancreatic cancer by supporting apoptotic resistance and angiogenesis. *Cancer Res.* **2012**, *72*, 4829-4839.
- (62) Tasaki, M.; Shimada, K.; Kimura, H.; Tsujikawa, K.; Konishi, N. ALKBH3, a human AlkB homologue, contributes to cell survival in human non-small-cell lung cancer. *Br. J. Cancer* **2011**, *104*, 700-706.
- (63) Hotta, K.; Sho, M.; Fujimoto, K.; Shimada, K.; Yamato, I.; Anai, S.; Harada, H.; Tsujikawa, K.; Konishi, N.; Shinohara, N.; Nakajima, Y. Clinical significance and therapeutic potential of prostate cancer

- antigen-1/ALKBH3 in human renal cell carcinoma. *Oncol. Rep.* **2015**, *34*, 648-654.
- (64) Walker, A. R.; Silvestrov, P.; Müller, T. A.; Podolsky, R. H.; Dyson, G.; Hausinger, R. P.; Cisneros, G. A. ALKBH7 variant related to prostate cancer exhibits altered substrate binding. *PLoS Comput. Biol.* **2017**, *13*, e1005345.
- (65) Ohshio, I.; Kawakami, R.; Tsukada, Y.; Nakajima, K.; Kitae, K.; Shimanoe, T.; Saigo, Y.; Hase, H.; Ueda, Y.; Jingushi, K.; Tsujikawa, K. ALKBH8 promotes bladder cancer growth and progression through regulating the expression of survivin. *Biochem. Biophys. Res. Commun.* **2016**, *477*, 413-418.
- (66) Shimada, K.; Nakamura, M.; Anai, S.; De Velasco, M.; Tanaka, M.; Tsujikawa, K.; Ouji, Y.; Konishi, N. A novel human AlkB homologue, ALKBH8, contributes to human bladder cancer progression. *Cancer Res.* **2009**, *69*, 3157-3164.
- (67) Xie, L. J.; Liu, L.; Cheng, L. Selective inhibitors of AlkB family of nucleic acid demethylases. *Biochem.* **2020**, *59*, 230-239.
- (68) Schofield, C. J.; Zhang, Z. Structural and mechanistic studies on 2-oxoglutarate-dependent oxygenases and related enzymes. *Curr. Opin. Struct. Biol.* **1999**, *9*, 722-731.
- (69) Martinez, S.; Hausinger, R. P. Catalytic mechanisms of Fe(II)- and 2-oxoglutarate-dependent oxygenases. *J. Biol. Chem.* **2015**, *290*, 20702-20711.
- (70) Zhu, C.; Yi, C. Switching demethylation activities between AlkB family RNA/DNA demethylases through exchange of active-site residues. *Angew. Chem. Int. Ed.* **2014**, *53*, 3659-3662.
- (71) Holland, P. J.; Hollis, T. Structural and mutational analysis of *Escherichia coli* AlkB provides insight into substrate specificity and DNA damage searching. *PLoS One* **2010**, *5*, e8680.
- (72) Rabe, P.; Beale, J. H.; Butryn, A.; Aller, P.; Dirr, A.; Lang, P. A.; Axford, D. N.; Carr, S. B.; Leissing, T. M.; McDonough, M. A.; Davy, B.; Ebrahim, A.; Orleans, J.; Storm, S. L. S.; Orville, A. M.; Schofield, C. J.; Owen, R. L. Anaerobic fixed-target serial crystallography. *IUCr* **2020**, *7*, 901-912.
- (73) Yu, B.; Hunt, J. F. Enzymological and structural studies of the mechanism of promiscuous substrate recognition by the oxidative DNA repair enzyme AlkB. *Proc. Natl. Acad. Sci. U.S.A.* **2009**, *106*, 14315-14320.
- (74) Li, H.; Zhang, Y.; Guo, Y.; Liu, R.; Yu, Q.; Gong, L.; Liu, Z.; Xie, W.; Wang, C. ALKBH1 promotes lung cancer by regulating m6A RNA demethylation. *Biochem. Pharmacol.* **2021**, *189*, 114284.
- (75) Chen, B.; Gan, J.; Yang, C. The complex structures of ALKBH2 mutants cross-linked to dsDNA reveal the conformational swing of β -hairpin. *Sci. China Chem.* **2014**, *57*, 307-313.
- (76) Yi, C.; Chen, B.; Qi, B.; Zhang, W.; Jia, G.; Zhang, L.; Li, C. J.; Dinner, A. R.; Yang, C. G.; He, C. Duplex interrogation by a direct DNA repair protein in search of base damage. *Nat. Struct. Mol. Biol.* **2012**, *19*, 671-676.
- (77) Lu, L.; Yi, C.; Jian, X.; Zheng, G.; He, C. Structure determination of DNA methylation lesions N1-meA and N3-meC in duplex DNA using a cross-linked protein-DNA system. *Nucleic Acids Research* **2010**, *38*, 4415-4425.
- (78) Sundheim, O.; Vågbo, C. B.; Bjørås, M.; Sousa, M. M. L.; Talstad, V.; Aas, P. A.; Drabløs, F.; Krokan, H. E.; Tainer, J. A.; Slupphaug, G. Human ABH3 structure and key residues for oxidative demethylation to reverse DNA/RNA damage. *EMBO J.* **2006**, *25*, 3389-3397.
- (79) Pastore, C.; Topalidou, I.; Forouhar, F.; Yan, A. C.; Levy, M.; Hunt, J. F. Crystal structure and RNA binding properties of the RNA recognition motif (RRM) and AlkB domains in human AlkB homologue 8 (ABH8), an enzyme catalyzing tRNA hypermodification. *J. Biol. Chem.* **2012**, *287*, 2130-2143.
- (80) Zhang, X.; Wei, L. H.; Wang, Y.; Xiao, Y.; Liu, J.; Zhang, W.; Yan, N.; Amu, G.; Tang, X.; Zhang, L.; Jia, G. Structural insights into FTO's catalytic mechanism for the demethylation of multiple RNA substrates. *Proc. Natl. Acad. Sci. U.S.A.* **2019**, *116*, 2919-2924.
- (81) Aik, W.; McDonough, M. A.; Thalhammer, A.; Chowdhury, R.; Schofield, C. J. Role of the jelly-roll fold in substrate binding by 2-oxoglutarate oxygenases. *Curr. Opin. Struct. Biol.* **2012**, *22*, 691-700.
- (82) Aik, W.; Scotti, J. S.; Choi, H.; Gong, L.; Demetriades, M.; Schofield, C. J.; McDonough, M. A. Structure of human RNA N⁶-methyladenine demethylase ALKBH5 provides insights into its mechanisms of nucleic acid recognition and demethylation. *Nucleic Acids Research* **2014**, *42*, 4741-4754.
- (83) Ergel, B.; Gill, M. L.; Brown, L.; Yu, B.; Palmer, A. G., 3rd; Hunt, J. F. Protein dynamics control the progression and efficiency of the catalytic reaction cycle of the *Escherichia coli* DNA-repair enzyme AlkB. *J. Biol. Chem.* **2014**, *289*, 29584-29601.
- (84) Yang, C. G.; Yi, C.; Duguid, E. M.; Sullivan, C. T.; Jian, X.; Rice, P. A.; He, C. Crystal structures of DNA/RNA repair enzymes AlkB and ABH2 bound to dsDNA. *Nature* **2008**, *452*, 961-965.
- (85) Yu, B.; Edstrom, W. C.; Benach, J.; Hamuro, Y.; Weber, P. C.; Gibney, B. R.; Hunt, J. F. Crystal structures of catalytic complexes of the oxidative DNA/RNA repair enzyme AlkB. *Nature* **2006**, *439*, 879-884.
- (86) Han, Z.; Niu, T.; Chang, J.; Lei, X.; Zhao, M.; Wang, Q.; Cheng, W.; Wang, J.; Feng, Y.; Chai, J. Crystal structure of the FTO protein reveals basis for its substrate specificity. *Nature* **2010**, *464*, 1205-1209.
- (87) Zhang, L.-S.; Xiong, Q.-P.; Peña Perez, S.; Liu, C.; Wei, J.; Le, C.; Zhang, L.; Harada, B. T.; Dai, Q.; Feng, X.; Hao, Z.; Wang, Y.; Dong, X.; Hu, L.; Wang, E.-D.; Pan, T.; Klungland, A.; Liu, R.-J.; He, C. ALKBH7-mediated demethylation regulates mitochondrial polycistronic RNA processing. *Nat. Cell Biol.* **2021**, *23*, 684-691.
- (88) Solberg, A.; Robertson, A. B.; Aronsen, J. M.; Rognmo, Ø.; Sjaastad, I.; Wisløff, U.; Klungland, A. Deletion of mouse Alkbh7 leads to obesity. *J. Mol. Cell Biol.* **2013**, *5*, 194-203.
- (89) Songe-Møller, L.; van den Born, E.; Leihne, V.; Vågbo, C. B.; Kristoffersen, T.; Krokan, H. E.; Kirpekar, F.; Falnes, P.; Klungland, A. Mammalian ALKBH8 possesses tRNA methyltransferase activity required for the biogenesis of multiple wobble uridine modifications implicated in translational decoding. *Mol. Cell Biol.* **2010**, *30*, 1814-1827.
- (90) Grzyska, P. K.; Appelman, E. H.; Hausinger, R. P.; Proshlyakov, D. A. Insight into the mechanism of an iron dioxygenase by resolution of steps following the FeIV=HO species. *Proc. Natl. Acad. Sci. U.S.A.* **2010**, *107*, 3982-3987.
- (91) Elkins, J. M.; Hewitson, K. S.; McNeill, L. A.; Seibel, J. F.; Schlemminger, I.; Pugh, C. W.; Ratcliffe, P. J.; Schofield, C. J. Structure of factor-inhibiting hypoxia-inducible factor (HIF) reveals mechanism of oxidative modification of HIF-1 alpha. *J. Biol. Chem.* **2003**, *278*, 1802-1806.
- (92) Zhang, Z.; Ren, J.; Stammers, D. K.; Baldwin, J. E.; Harlos, K.; Schofield, C. J. Structural origins of the selectivity of the trifunctional oxygenase clavaminic acid synthase. *Nat. Struct. Biol.* **2000**, *7*, 127-133.
- (93) Krebs, C.; Galonić Fujimori, D.; Walsh, C. T.; Bollinger, J. M. Non-heme Fe(IV)-oxo intermediates. *Acc. Chem. Res.* **2007**, *40*, 484-492.
- (94) Mishina, Y.; He, C. Oxidative dealkylation DNA repair mediated by the mononuclear non-heme iron AlkB proteins. *J. Inorg. Biochem.* **2006**, *100*, 670-678.
- (95) Borowski, T.; Bassan, A.; Siegbahn, P. E. Mechanism of dioxygen activation in 2-oxoglutarate-dependent enzymes: a hybrid DFT study. *Chemistry* **2004**, *10*, 1031-1041.
- (96) Zhou, J.; Kelly, W. L.; Bachmann, B. O.; Gunsior, M.; Townsend, C. A.; Solomon, E. I. Spectroscopic studies of substrate interactions with clavaminic acid synthase 2, a multifunctional alpha-KG-dependent non-heme iron enzyme: correlation with mechanisms and reactivities. *J. Am. Chem. Soc.* **2001**, *123*, 7388-7398.
- (97) Sedgwick, B. Repairing DNA-methylation damage. *Nat. Rev. Mol. Cell Biol.* **2004**, *5*, 148-157.
- (98) Hausinger, R. P. FeII/alpha-ketoglutarate-dependent hydroxylases and related enzymes. *Crit. Rev. Biochem. Mol. Biol.* **2004**, *39*, 21-68.

- (99) Lu, L.; Zhu, C.; Xia, B.; Yi, C. Oxidative demethylation of DNA and RNA mediated by non-heme iron-dependent dependent oxygenases. *Chem. Asian. J.* **2014**, *9*, 2018-2029.
- (100) de Visser, S. P. Mechanistic insight on the activity and substrate selectivity of nonheme iron dependent oxygenases. *Chem. Rec.* **2018**, *18*, 1501-1516.
- (101) Alemu, E.; He, C.; Klungland, A. ALKBHs-facilitated RNA modifications and de-modifications. *DNA Repair (Amst)* **2016**, *44*, 87-91.
- (102) Boriack-Sjodin, P. A.; Ribich, S.; Copeland, R. A. RNA-modifying proteins as anticancer drug targets. *Nat. Rev. Drug Discov.* **2018**, *17*, 435-453.
- (103) Demetriades, M.; Leung, I. K. H.; Chowdhury, R.; Chan, M. C.; McDonough, M. A.; Yeoh, K. K.; Tian, Y.-M.; Claridge, T.; Ratcliffe, P. J.; Woon, E. C. Y.; Schofield, C. J. Dynamic combinatorial chemistry employing boronic acids/boronate esters leads to potent oxygenase inhibitors. *Angew. Chem. Int. Ed.* **2012**, *51*, 6672-6675.
- (104) Woon, E. C. Y.; Tumber, A.; Kawamura, A.; Hillringhaus, L.; Ge, W.; Rose, N. R.; Ma, J. H. Y.; Chan, M. C.; Walport, L. J.; Che, K. H.; Ng, S. S.; Marsden, B. D.; Oppermann, U.; McDonough, M. A.; Schofield, C. J. Linking of 2-oxoglutarate and substrate binding sites enables potent and highly selective inhibition of JmjC histone demethylases. *Angew. Chem. Int. Ed.* **2012**, *51*, 1631-1634.
- (105) Suzuki, T.; Miyata, N. Lysine demethylases inhibitors. *J. Med. Chem.* **2011**, *54*, 8236-8250.
- (106) Toh, J. D. W.; Sun, L.; Lau, L. Z. M.; Tan, J.; Low, J. J. A.; Tang, C. W. Q.; Cheong, E. J. Y.; Tan, M. J. H.; Chen, Y.; Hong, W.; Gao, Y. G.; Woon, E. C. Y. A strategy based on nucleotide specificity leads to a subfamily-selective and cell-active inhibitor of N(6)-methyladenosine demethylase FTO. *Chem. Sci.* **2015**, *6*, 112-122.
- (107) Huang, Y.; Su, R.; Sheng, Y.; Dong, L.; Dong, Z.; Xu, H.; Ni, T.; Zhang, Z. S.; Zhang, T.; Li, C.; Han, L.; Zhu, Z.; Lian, F.; Wei, J.; Deng, Q.; Wang, Y.; Wunderlich, M.; Gao, Z.; Pan, G.; Zhong, D.; Zhou, H.; Zhang, N.; Gan, J.; Jiang, H.; Mulloy, J. C.; Qian, Z.; Chen, J.; Yang, C. G. Small-molecule targeting of oncogenic FTO demethylase in acute myeloid leukemia. *Cancer Cell* **2019**, *35*, 677-691.
- (108) Jaakkola, P.; Mole, D. R.; Tian, Y. M.; Wilson, M. I.; Gielbert, J.; Gaskell, S. J.; von Kriegsheim, A.; Hebestreit, H. F.; Mukherji, M.; Schofield, C. J.; Maxwell, P. H.; Pugh, C. W.; Ratcliffe, P. J. Targeting of HIF- α to the von Hippel-Lindau ubiquitylation complex by O₂-regulated prolyl hydroxylation. *Science* **2001**, *292*, 468-472.
- (109) Schofield, C. J.; Ratcliffe, P. J. Oxygen sensing by HIF hydroxylases. *Nat. Rev. Mol. Cell. Biol.* **2004**, *5*, 343-354.
- (110) Conejo-Garcia, A.; McDonough, M. A.; Loenarz, C.; McNeill, L. A.; Hewitson, K. S.; Ge, W.; Liénard, B. M.; Schofield, C. J.; Clifton, I. J. Structural basis for binding of cyclic 2-oxoglutarate analogues to factor-inhibiting hypoxia-inducible factor. *Bioorg. Med. Chem. Lett.* **2010**, *20*, 6125-6128.
- (111) Al-Qahtani, K.; Jabeen, B.; Sekirnik, R.; Riaz, N.; Claridge, T.; Schofield, C.; McCullagh, J. The broad spectrum 2-oxoglutarate oxygenase inhibitor N-oxalylglycine is present in rhubarb and spinach leaves. *Phytochem.* **2015**, *117*, 456-461.
- (112) Woon, E. C. Y.; Demetriades, M.; Bagg, E. A. L.; Aik, W.; Krylova, S. M.; Ma, J. H. Y.; Chan, M.; Walport, L. J.; Wegman, D. W.; Dack, K. N.; McDonough, M. A.; Krylov, S. N.; Schofield, C. J. Dynamic combinatorial mass spectrometry leads to inhibitors of a 2-oxoglutarate-dependent nucleic acid demethylase. *J. Med. Chem.* **2012**, *55*, 2173-2184.
- (113) Rose, N. R.; Woon, E. C.; Kingham, G. L.; King, O. N.; Mecnović, J.; Clifton, I. J.; Ng, S. S.; Talib-Hardy, J.; Oppermann, U.; McDonough, M. A.; Schofield, C. J. Selective inhibitors of the JMJD2 histone demethylases: combined nondenaturing mass spectrometric screening and crystallographic approaches. *J. Med. Chem.* **2010**, *53*, 1810-1818.
- (114) Aik, W.; Demetriades, M.; Hamdan, M. K. K.; Bagg, E. A. L.; Yeoh, K. K.; Lejeune, C.; Zhang, Z.; McDonough, M. A.; Schofield, C. J. Structural basis for inhibition of the fat mass and obesity associated protein (FTO). *J. Med. Chem.* **2013**, *56*, 3680-3688.
- (115) Shi, R.; Mullins, E. A.; Shen, X. X.; Lay, K. T.; Yuen, P. K.; David, S. S.; Rokas, A.; Eichman, B. F. Selective base excision repair of DNA damage by the non-base-flipping DNA glycosylase AlkC. *EMBO J.* **2018**, *37*, 63-74.
- (116) Koivunen, P.; Hirsilä, M.; Remes, A. M.; Hassinen, I. E.; Kivirikko, K. I.; Myllyharju, J. Inhibition of hypoxia-inducible factor (HIF) hydroxylases by citric acid cycle intermediates: possible links between cell metabolism and stabilization of HIF. *J. Biol. Chem.* **2007**, *282*, 4524-4532.
- (117) Rose, N. R.; McDonough, M. A.; King, O. N.; Kawamura, A.; Schofield, C. J. Inhibition of 2-oxoglutarate dependent oxygenases. *Chem. Soc. Rev.* **2011**, *40*, 4364-4397.
- (118) Yi, C.; Jia, G.; Hou, G.; Dai, Q.; Zhang, W.; Zheng, G.; Jian, X.; Yang, C. G.; Cui, Q.; He, C. Iron-catalysed oxidation intermediates captured in a DNA repair dioxygenase. *Nature* **2010**, *468*, 330-333.
- (119) Chen, W.; Zhang, L.; Zheng, G.; Fu, Y.; Ji, Q.; Liu, F.; Chen, H.; He, C. Crystal structure of the RNA demethylase ALKBH5 from zebrafish. *FEBS Lett.* **2014**, *588*, 892-898.
- (120) Couture, J. F.; Collazo, E.; Ortiz-Tello, P. A.; Brunzelle, J. S.; Trievel, R. C. Specificity and mechanism of JMJD2A, a trimethyllysine-specific histone demethylase. *Nat. Struct. Mol. Biol.* **2007**, *14*, 689-695.
- (121) Hewitson, K. S.; Liénard, B. M.; McDonough, M. A.; Clifton, I. J.; Butler, D.; Soares, A. S.; Oldham, N. J.; McNeill, L. A.; Schofield, C. J. Structural and mechanistic studies on the inhibition of the hypoxia-inducible transcription factor hydroxylases by tricarboxylic acid cycle intermediates. *J. Biol. Chem.* **2007**, *282*, 3293-3301.
- (122) Chen, F.; Bian, K.; Tang, Q.; Fedeles, B. I.; Singh, V.; Humulock, Z. T.; Essigmann, J. M.; Li, D. Oncometabolites D- and L-2-hydroxyglutarate inhibit the AlkB family DNA repair enzymes under physiological conditions. *Chem. Res. Toxicol.* **2017**, *30*, 1102-1110.
- (123) Chowdhury, R.; Yeoh, K. K.; Tian, Y. M.; Hillringhaus, L.; Bagg, E. A.; Rose, N. R.; Leung, I. K.; Li, X. S.; Woon, E. C.; Yang, M.; McDonough, M. A.; King, O. N.; Clifton, I. J.; Klose, R. J.; Claridge, T. D.; Ratcliffe, P. J.; Schofield, C. J.; Kawamura, A. The oncometabolite 2-hydroxyglutarate inhibits histone lysine demethylases. *EMBO Rep.* **2011**, *12*, 463-469.
- (124) Welford, R. W.; Schlemminger, I.; McNeill, L. A.; Hewitson, K. S.; Schofield, C. J. The selectivity and inhibition of AlkB. *J. Biol. Chem.* **2003**, *278*, 10157-10161.
- (125) Eniafe, J.; Jiang, S. The functional roles of TCA cycle metabolites in cancer. *Oncogene* **2021**, *40*, 3351-3363.
- (126) Hopkinson, R. J.; Tumber, A.; Yapp, C.; Chowdhury, R.; Aik, W.; Che, K. H.; Li, X. S.; Kristensen, J. B. L.; King, O. N. F.; Chan, M. C.; Yeoh, K. K.; Choi, H.; Walport, L. J.; Thinnies, C. C.; Bush, J. T.; Lejeune, C.; Rydzik, A. M.; Rose, N. R.; Bagg, E. A.; McDonough, M. A.; Krojer, T.; Yue, W. W.; Ng, S. S.; Olsen, L.; Brennan, P. E.; Oppermann, U.; Muller-Knapp, S.; Klose, R. J.; Ratcliffe, P. J.; Schofield, C. J.; Kawamura, A. 5-Carboxy-8-hydroxyquinoline is a broad spectrum 2-oxoglutarate oxygenase inhibitor which causes iron translocation. *Chem. Sci.* **2013**, *4*, 3110-3117.
- (127) Karkhanina, A. A.; Mecnović, J.; Musheev, M. U.; Krylova, S. M.; Petrov, A. P.; Hewitson, K. S.; Flashman, E.; Schofield, C. J.; Krylov, S. N. Direct analysis of enzyme-catalysed DNA demethylation. *Anal. Chem.* **2009**, *81*, 5871-5875.
- (128) Rose, N. R.; Ng, S. S.; Mecnović, J.; Liénard, B. M.; Bello, S. H.; Sun, Z.; McDonough, M. A.; Oppermann, U.; Schofield, C. J. Inhibitor scaffolds for 2-oxoglutarate-dependent histone lysine demethylases. *J. Med. Chem.* **2008**, *51*, 7053-7056.
- (129) Li, F.; Kennedy, S.; Hajian, T.; Gibson, E.; Seitova, A.; Xu, C.; Arrowsmith, C. H.; Vedadi, M. A radioactivity-based assay for screening human m6A-RNA methyltransferase, METTL3-METTL14 complex, and demethylase ALKBH5. *J. Biomol. Screen* **2016**, *21*, 290-297.
- (130) Leung, I. K.; Demetriades, M.; Hardy, A. P.; Lejeune, C.; Smart, T. J.; Szöllösi, A.; Kawamura, A.; Schofield, C. J.; Claridge, T. D. Reporter ligand NMR screening method for 2-oxoglutarate oxygenase inhibitors. *J. Med. Chem.* **2013**, *56*, 547-555.

- (131) England, K. S.; Tumber, A.; Krojer, T.; Scozzafava, G.; Ng, S. S.; Daniel, M.; Szykowska, A.; Che, K.; von Delft, F.; Burgess-Brown, N. A.; Kawamura, A.; Schofield, C. J.; Brennan, P. E. Optimisation of a triazolopyridine based histone demethylase inhibitor yields a potent and selective KDM2A (FBXL11) inhibitor. *Med. Chem. Comm.* **2014**, *5*, 1879-1886.
- (132) Schofield, C. J.; Ratcliffe, P. J. Oxygen sensing by HIF hydroxylases. *Nat. Rev. Mol. Cell Biol.* **2004**, *5*, 343-354.
- (133) Yan, L.; Colandrea, V. J.; Hale, J. J. Prolyl hydroxylase domain-containing protein inhibitors as stabilisers of hypoxia-inducible factor: small molecule-based therapeutics for anemia. *Expert Opin. Ther. Pat.* **2010**, *20*, 1219-1245.
- (134) Hong, Y. R.; Kim, H. T.; Lee, S. C.; Ro, S.; Cho, J. M.; Kim, I. S.; Jung, Y. H. [(4-Hydroxyl-benzo[4,5]thieno[3,2-c]pyridine-3-carbonyl)-amino]-acetic acid derivatives; HIF prolyl 4-hydroxylase inhibitors as oral erythropoietin secretagogues. *Bioorg. Med. Chem. Lett.* **2013**, *23*, 5953-5957.
- (135) Bernhardt, W. M.; Wiesener, M. S.; Scigalla, P.; Chou, J.; Schmieder, R. E.; Günzler, V.; Eckardt, K.-U. Inhibition of prolyl hydroxylases increases erythropoietin production in ESRD. *J. Am. Soc. Nephrol.* **2010**, *21*, 2151-2156.
- (136) Das, M.; Yang, T.; Dong, J.; Prasetya, F.; Xie, Y.; Wong, K. H. Q.; Cheong, A.; Woon, E. C. Y. Multiprotein dynamic combinatorial chemistry: a strategy for the simultaneous discovery of subfamily-selective inhibitors for nucleic acid demethylases FTO and ALKBH3. *Chem. Asian J.* **2018**, *13*, 2854-2867.
- (137) Zhou, Y.-X.; Xia, W.; Yue, W.; Peng, C.; Rahman, K.; Zhang, H. Rhein: a review of pharmacological activities. *eCAM* **2015**, Article ID 578107.
- (138) Chen, B.; Ye, F.; Yu, L.; Jia, G.; Huang, X.; Zhang, X.; Peng, S.; Chen, K.; Wang, M.; Gong, S.; Zhang, R.; Yin, J.; Li, H.; Yang, Y.; Liu, H.; Zhang, J.; Zhang, H.; Zhang, A.; Jiang, H.; Luo, C.; Yang, C. G. Development of cell-active N6-methyladenosine RNA demethylase FTO inhibitor. *J. Am. Chem. Soc.* **2012**, *134*, 17963-17971.
- (139) Svensen, N.; Jaffrey, S. R. Fluorescent RNA aptamers as a tool to study RNA-modifying enzymes. *Cell Chem. Biol.* **2016**, *23*, 415-425.
- (140) Li, Q.; Huang, Y.; Liu, X.; Gan, J.; Chen, H.; Yang, C.-G. Rhein inhibits AlkB repair enzymes and sensitizes cells to methylated DNA damage. *J. Biol. Chem.* **2016**, *291*, 11083-11093.
- (141) Huang, Y.; Yan, J.; Li, Q.; Li, J.; Gong, S.; Zhou, H.; Gan, J.; Jiang, H.; Jia, G.-F.; Luo, C.; Yang, C.-G. Meclofenamic acid selectively inhibits FTO demethylation of m6A over ALKBH5. *Nucleic Acids Research* **2015**, *43*, 373-384.
- (142) Whitehouse, M. W. Drugs to treat inflammation: a historical introduction. *Curr. Med. Chem.* **2005**, *12* (25), 2931-2942.
- (143) Wang, T.; Hong, T.; Huang, Y.; Su, H.; Wu, F.; Chen, Y.; Wei, L.; Huang, W.; Hua, X.; Xia, Y.; Xu, J.; Gan, J.; Yuan, B.; Feng, Y.; Zhang, X.; Yang, C. G.; Zhou, X. Fluorescein derivatives as bifunctional molecules for the simultaneous inhibiting and labeling of FTO protein. *J. Am. Chem. Soc.* **2015**, *137*, 13736-13739.
- (144) He, W.; Zhou, B.; Liu, W.; Zhang, M.; Shen, Z.; Han, Z.; Jiang, Q.; Yang, Q.; Song, C.; Wang, R.; Niu, T.; Han, S.; Zhang, L.; Wu, J.; Guo, F.; Zhao, R.; Yu, W.; Chai, J.; Chang, J. Identification of a novel small-molecule binding site of the fat mass and obesity associated protein (FTO). *J. Med. Chem.* **2015**, *58*, 7341-7348.
- (145) Qiao, Y.; Zhou, B.; Zhang, M.; Liu, W.; Han, Z.; Song, C.; Yu, W.; Yang, Q.; Wang, R.; Wang, S.; Shi, S.; Zhao, R.; Chai, J.; Chang, J. A novel inhibitor of the obesity-related protein FTO. *Biochemistry* **2016**, *55*, 1516-1522.
- (146) Wang, R.; Zhifu, H.; Liu, B.; Zhou, B.; Wang, N.; Jiang, Q.; Qiao, Y.; Song, C.; Chai, J.; Chang, J. Identification of natural compound radicicol as a potent FTO inhibitor. *Mol. Pharmaceutics* **2018**, *15*, 4092-4098.
- (147) Peng, S.; Xiao, W.; Ju, D.; Sun, B.; Hou, N.; Liu, Q.; Wang, Y.; Zhao, H.; Gao, C.; Zhang, S.; Cao, R.; Li, P.; Huang, H.; Ma, Y.; Wang, Y.; Lai, W.; Ma, Z.; Zhang, W.; Huang, S.; Wang, H.; Zhang, Z.; Zhao, L.; Cai, T.; Zhao, Y.-L.; Wang, F.; Nie, Y.; Zhi, G.; Yang, Y.-G.; Zhang, E.; Huang, N. Identification of entacapone as a chemical inhibitor of FTO mediating metabolic regulation through FOXO1. *Sci. Transl. Med.* **2019**, *11*, eaau7116.
- (148) Cao, R.; Liu, M.; Yin, M.; Liu, Q.; Wang, Y.; Huang, N. Discovery of novel tubulin inhibitors via structure-based hierarchical virtual screening. *J. Chem. Inf. Model.* **2012**, *52*, 2730-2740.
- (149) Niu H.; Gang Z.; Jijie C.; Shiming P.; Nannan Hou.; Entacapone for prevention and treatment of obesity and related metabolic diseases. International Patent Application WO/201408254-A1, 2014; National Institute of Biological Sciences Beijing.
- (150) Shimada, K.; Nakamura, M.; Ishida, E.; Higuchi, T.; Yamamoto, H.; Tsujikawa, K.; Konishi, N. Prostate cancer antigen-1 contributes to cell survival and invasion through discoidin receptor 1 in human prostate cancer. *Cancer Sci.* **2008**, *99*, 39-45.
- (151) Nakao, S.; Mabuchi, M.; Shimizu, T.; Itoh, Y.; Takeuchi, Y.; Ueda, M.; Mizuno, H.; Shigi, N.; Ohshio, I.; Jinguji, K.; Ueda, Y.; Yamamoto, M.; Furukawa, T.; Aoki, S.; Tsujikawa, K.; Tanaka, A. Design and synthesis of prostate cancer antigen-1 (PCA-1/ALKBH3) inhibitors as anti-prostate cancer drugs. *Bioorg. Med. Chem. Lett.* **2014**, *24*, 1071-1074.
- (152) Ueda, M.; Shimizu, T.; Mabuchi, M.; Horiike, K.; Kitae, K.; Hase, H.; Ueda, Y.; Tsujikawa, K.; Tanaka, A. Novel metabolically stable PCA-1/ALKBH3 inhibitor has potent antiproliferative effects on DU145 cells in vivo. *Anticancer Res.* **2018**, *38*, 211-218.
- (153) Nigam, R.; Babu, K. R.; Ghosh, T.; Kumari, B.; Akula, D.; Rath, S. N.; Das, P.; Anindya, R.; Khan, F. A. Indenone derivatives as inhibitor of human DNA dealkylation repair enzyme AlkBH3. *Bioorg. Med. Chem.* **2018**, *26*, 4100-4112.
- (154) Nigam, R.; Raveendra Babu, K.; Ghosh, T.; Kumari, B.; Das, P.; Anindya, R.; Ahmed Khan, F. Synthesis of 2-chloro-3-amino indenone derivatives and their evaluation as inhibitors of DNA dealkylation repair. *Chem. Biol. Drug Des.* **2021**, *97*, 1170-1184.
- (155) Zheng, G.; Cox, T.; Tribbey, L.; Wang, G. Z.; Iacoban, P.; Boother, M. E.; Gabriel, G. J.; Zhou, L.; Bae, N.; Rowles, J.; He, C.; Olsen, M. J. Synthesis of a FTO inhibitor with anticonvulsant activity. *ACS Chem. Neurosci.* **2014**, *5*, 658-665.
- (156) Wang, Y.; Li, J.; Han, X.; Wang, N.; Song, C.; Wang, R.; Chang, J. Identification of Clausine E as an inhibitor of fat mass and obesity-associated protein (FTO) demethylase activity. *J. Mol. Recognit.* **2019**, *32*, e2800.
- (157) Li, J.; Wang, Y.; Han, X.; Wang, N.; Yu, W.; Wang, R.; Chang, J. The role of chlorine atom on the binding between 2-phenyl-1H-benzimidazole analogues and fat mass and obesity-associated protein. *J. Mol. Recognit.* **2018**, *32*, e2774.
- (158) Li, N.; Kang, Y.; Wang, L.; Huff, S.; Tang, R.; Hui, H.; Agrawal, K.; Gonzalez, G. M.; Wang, Y.; Patel, S. P.; Rana, T. M. ALKBH5 regulates anti-PD-1 therapy response by modulating lactate and suppressive immune cell accumulation in tumor microenvironment. *PNAS* **2020**, *117*, 20159-20170.
- (159) Malacrida, A.; Rivara, M.; Domizio, A. D.; Cislighi, G.; Miloso, M.; Zuliani, V.; Nicolini, G. 3D proteome-wide screening and activity evaluation of a new ALKBH5 inhibitor in U87 glioblastoma cell line. *Bioorg. Med. Chem.* **2020**, *28*, 115300.
- (160) Selberg, S.; Seli, N.; Kankuri, E.; Karelson, M. Rational design of novel anticancer small-molecule RNA m6A demethylase ALKBH5 inhibitors. *ACS Omega* **2021**, *6*, 13310-13320.
- (161) Laird, P. W. Principles and challenges of genomewide DNA methylation analysis. *Nat. Rev. Genet.* **2010**, *11*, 191-203.
- (162) Bock, C.; Tomazou, E. M.; Brinkman, A. B.; Muller, F.; Simmer, F.; Gu, H.; Jäger, N.; Gnirke, A.; Stunnenberg, H. G.; Meissner, A. Quantitative comparison of genome-wide DNA methylation mapping technologies. *Nat. Biotechnol.* **2010**, *28*, 1106-1114.
- (163) Dominissini, D.; Moshitch-Moshkovitz, S.; Schwartz, S.; Salmon-Divon, M.; Ungar, L.; Osenberg, S.; Cesarkas, K.; Jacob-Hirsch, J.; Amariglio, N.; Kupiec, M.; Sorek, R.; Rechavi, G. Topology of the human and mouse m6A RNA methylomes revealed by m6A-seq. *Nature* **2012**, *485*, 201-206.

- (164) Meyer, K. D.; Saletore, Y.; Zumbo, P.; Elemento, O.; Mason, C. E.; Jaffrey, S. R. Comprehensive analysis of mRNA methylation reveals enrichment in 3' UTRs and near stop codons. *Cell* **2012**, *149*, 1635-1646.
- (165) Linder, B.; Grozhik, A. V.; Olarerin-George, A. O.; Meydan, C.; Mason, C. E.; Jaffrey, S. R. Single-nucleotide-resolution mapping of m6A and m6Am throughout the transcriptome. *Nat. Methods* **2015**, *12*, 767-772.
- (166) Dominissini, D.; Nachtergaele, S.; Moshitch-Moshkovitz, S.; Peer, E.; Kol, N.; Ben-Haim, S.; Dai, Q.; Segni, A. D.; Salmon-Divon, M.; Wesley, C. C.; Guanqun, Z.; Pan, T.; Solomon, O.; Eyal, E.; Hershkovitz, V.; Han, D.; Doré, L. C.; Amariglio, N.; Rechavi, G.; He, C. The dynamic N¹-methyladenosine methylome in eukaryotic messenger RNA. *Nature* **2016**, *530*, 441-446.
- (167) Delatte, B.; Wang, F.; Ngoc L. V.; Collignon, E.; Bonvin, E.; Deplus, R.; Calonne, E.; Hassabi, B.; Putmans, P.; Awe, S.; Wetzels, C.; Kreher, J.; Soin, R.; Creppe, C.; Limbach, P. A.; Gueydan, C.; Kruijs, V.; Brehm, A.; Minakina, S.; Defrance, M.; Steward, R.; Fuks, F. *Science* **2016**, *351*, 282-285.
- (168) Zhang, L. S.; Liu, C.; Ma, H.; Dai, Q.; Sun, H. L.; Luo, G.; Zhang, Z.; Zhang, L.; Hu, L.; Dong, X.; He, C. Transcriptome-wide mapping of internal N⁷-methylguanosine methylome in mammalian mRNA. *Mol. Cell* **2019**, *74*, 1304-1316.
- (169) Dai, Q.; Moshitch-Moshkovitz, S.; Han, D.; Kol, N.; Amariglio, N.; Rechavi, G.; Dominissini, D.; He, C. Nm-seq maps 2'-O-methylation sites in human mRNA with base precision. *Nat. Methods* **2017**, *14*, 695-698.
- (170) Roy, T. W.; Bhagwat, A. S. Kinetic studies of Escherichia coli AlkB using a new fluorescence-based assay for DNA methylation. *Nucleic Acids Research* **2007**, *35*, e147-e147.
- (171) Yang, T.; Cheong, A.; Mai, X.; Zou, S.; Woon, E. C. Y. A methylation-switchable conformational probe for the sensitive and selective detection of RNA demethylase activity. *Chem. Commun.* **2016**, *52*, 6181-6184.
- (172) Ueda, Y.; Kitae, K.; Ooshio, I.; Fusamae, Y.; Kawaguchi, M.; Jinguishi, K.; Harada, K.; Hirata, K.; Tsujikawa, K. A real-time PCR-based quantitative assay for 3-methylcytosine demethylase activity of ALKBH3. *Biochem. Biophys. Rep.* **2016**, *5*, 476-481.
- (173) Alves, J.; Vidugiris, G.; Goueli, S. A.; Zegzouti, H. Bioluminescent high-throughput succinate detection method for monitoring the activity of JMJC histone demethylases and Fe(II)/2-oxoglutarate-dependent dioxygenases. *SLAS Discovery* **2017**, *23*, 242-254.
- (174) Wang, Y.; Katanski, C. D.; Watkins, C.; Pan, J. N.; Dai, Q.; Jiang, Z.; Pan, T. A high-throughput screening method for evolving a demethylase enzyme with improved and new functionalities. *Nucleic Acids Research* **2021**, *49*, e30-e30.
- (175) Cheong, A.; Low, J. J. A.; Lim, A.; Yen, P. M.; Woon, E. C. Y. A fluorescent methylation-switchable probe for highly sensitive analysis of FTO N⁶-methyladenosine demethylase activity in cells. *Chem. Sci.* **2018**, *9*, 7174-7185.
- (176) Yang, T.; Low, J. J. A.; Woon, E. C. Y. A general strategy exploiting m⁵C duplex-remodelling effect for selective detection of RNA and DNA m⁵C methyltransferase activity in cells. *Nucleic Acids Research.* **2020**, *48*, e5.

Table of Contents

